Robust Global Stabilization of the DC-DC Boost Converter via Hybrid Control

T.A.F. Theunisse, J. Chai, R.G. Sanfelice, *Senior Member, IEEE,* and W.P.M.H. Heemels, *Senior Member, IEEE*

***Abstract*—In this paper, we consider the modeling and (robust) control of a DC-DC boost converter. In particular, we derive a mathematical model consisting of a constrained switched differential inclusion that includes all possible modes of operation of the converter. The obtained model is carefully selected to be amenable for the study of various important robustness properties. For this model, we design a control algorithm that induces robust, global asymptotic stability of a desired output voltage value. The guaranteed robustness properties ensure proper operation of the converter in the presence of noise in the state, unmodeled dynamics, and spatial regularization to reduce the high rate of switching. The establishment of these properties is enabled by recent tools for the study of robust stability in hybrid systems. Simulations illustrating the main results are included.**

***Index Terms*—Boost converter, DC-DC converters, hybrid control, stability, robustness, stability.**

I. Introduction

THE increasing number of renewable energy sources and distributed generators requires new strategies for the operation and management of the electricity grid in order to maintain, and even to improve, the reliability and quality the power supplied. Power electronics play a key role in distributed generation and in integration of renewable sources into the electric grid [2]. A recent challenge for these systems is the unavoidable variability of the power obtained from renewable resources, which, in turn, demands conversion technology that robustly adapts to changes in the supplies and demands.

One type of converter that is widely used in energy conversion is the DC-DC Boost converter. This converter draws power from a DC voltage source and supplies power to a load at a higher DC voltage value. Different approaches have been employed in the literature for the analysis and the design of such converters. Arguably, the most popular method used to control such converters is Pulse-Width Modulation (PWM). In PWM-based controllers, the switch in the circuit is turned on at the beginning of each switching period and is turned off when the reference value is lower than a certain carrier signal [3]. The analysis and design of a PWM controller is typically carried out by averaging the two steady state configurations of the circuit, leading to a single differential equation model, see, e.g. [4]. More recently, a renewed interest in power converters has originated from the rise of switching/hybrid modeling paradigms [3], [5]–[13], and new perspectives on their control were proposed, including time-based switching, state-event triggered control, and optimization-based control.

In this paper, motivated by the need of converters that robustly adapt to changes in renewable energy systems, we consider the modeling and robust control of a DC-DC Boost converter. As a difference to previous approaches, in which models only capture steady state modes of operation (see, e.g., [6], [7]), we propose a model that includes all possible modes of operation of the converter, including the discontinuous conduction mode. In this way, our model captures both transient behavior and every possible state of the system. Our proposed model consists of a switching differential inclusion with constraints. Using hybrid systems tools, we study the properties induced by a controller that triggers switches of the differential inclusion based on the value of the internal current and output voltage of the converter as well as on the value of the discrete state of the controller (a logic variable). We formally prove that the controller we employ, which is inspired by the one first proposed in [7] and that was studied by simulations therein, induces robust, global asymptotic stability of a desired output voltage value. The robustness properties guarantee proper operation of the converter in the presence of small noise in the state, unmodeled dynamics, and spatial regularization to relax the rate of switching. To the best of our knowledge, these properties of the Boost converter have not been previously established in the literature. The recently developed tools for robust stability in hybrid systems [14] form the enabling techniques to achieve these important results.

The remainder of the paper is organized as follows. After introducing notation, the principles of operation of the Boost converter are discussed and our mathematical model is presented in Section II. A switching control law is presented in Section III. In Section IV, global asymptotic stability for the closed-loop system is proven. In addition, the results on robustness are also presented in Section IV. In Section V, simulations are performed to illustrate our results. Finally, concluding remarks are presented in Section VI.

Notation: $\mathbb{R}$ denotes the set of real numbers. $\mathbb{R}^n$ denotes the n-dimensional Euclidean space. $\mathbb{R}_{\geq 0}$ denotes the set of nonnegative real numbers, i.e., $\mathbb{R}_{\geq 0} = [0, \infty)$. $\mathbb{N}$ denotes the set of natural numbers including 0, i.e., $\mathbb{N} = \{0, 1, \dots\}$. $\mathbb{B}$ denotes the closed unit ball in a Euclidean space centered at the origin. Given a set S, ∂S denotes its boundary. Given a vector $x \in \mathbb{R}^n$, $|x|$ denotes its Euclidean vector norm, i.e. $|x| = \sqrt{\sum_{j=1}^{n} x_j^2}$. Given a set $K \subset \mathbb{R}^n$ and a point $x \in \mathbb{R}^n$, the distance from x to the set K is denoted by $|x|_K := \inf_{y \in K} |x - y|$. We use the notation $\overline{\text{co}}$ to denote the closed

T. A. F. Theunisse and W.P.M.H. are with the Control Systems Technology group in the Department of Mechanical Engineering, Eindhoven University of Technology, P.O. Box 513, 5600 MB Eindhoven, The Netherlands. Email: t.a.f.theunisse@student.tue.nl, m.heemels@tue.nl. The work of W.P.M.H. was partially supported by the European 7th Framework Network of Excellence Highly-complex and networked control systems (HYCON2) (grant agreement no. 257462).

J. Chai and R. G. Sanfelice are with the Department of Computer Engineering, University of California at Santa Cruz, 1156 High St. Santa Cruz, CA 95064. Email: jchai3@ucsc.edu, ricardo@ucsc.edu. The research by J. Chai and R. G. Sanfelice has been partially supported by the NSF CAREER Grant no. ECS-1150306 and by AFOSR Grant no. FA9550-12-1-0366.

A preliminary and much shorter version of this work was presented in the conference publication [1].

convex hull of a set. For l vectors $x_i \in \mathbb{R}^{n_i}$, $i = 1, 2, \ldots, l$, we denote the vector obtained by stacking all the vectors in one (column) vector $x \in \mathbb{R}^n$ with $n = n_1 + n_2 + \ldots + n_l$ by $(x_1, x_2, \ldots, x_l)$, i.e., $(x_1, x_2, \ldots, x_l) = [x_1^\top, x_2^\top, \ldots, x_l^\top]^\top$. A function $\alpha : \mathbb{R}_{\geq 0} \to \mathbb{R}_{\geq 0}$ is said to be of class $\mathcal{K}$ if it is continuous, zero at zero and strictly increasing. It is said to be of class $\mathcal{K}_\infty$ if it is of class $\mathcal{K}$ and it is unbounded. A function $\beta : \mathbb{R}_{\geq 0} \times \mathbb{R}_{\geq 0} \to \mathbb{R}_{\geq 0}$ is said to be of class $\mathcal{KL}$ if $\beta(\cdot, t)$ is of class $\mathcal{K}$ for each fixed $t \geq 0$ and $\beta(s, \cdot)$ is nonincreasing and satisfies $\lim_{t\to\infty} \beta(s, t) = 0$ for each fixed $s \geq 0$.

II. Modeling

In this section, we describe the principles of operation of the DC-DC Boost converter. Afterwards, we present a model covering all possible system modes.

A. Principles of operation

The DC-DC Boost converter is shown in Figure 1. The Boost circuit consists of a capacitor c, an ideal diode d, a DC voltage source E, an inductor L, a resistor R, and an ideal switch S. The voltage across the capacitor is denoted v_c, and the current through the inductor is denoted i_L. The purpose of the circuit is to draw power from the DC voltage source, and supply power to the load at a higher DC voltage value. This task is accomplished by first closing the switch to store energy in the inductor, and then opening the switch to transfer that energy to the capacitor, where it is available to the load.

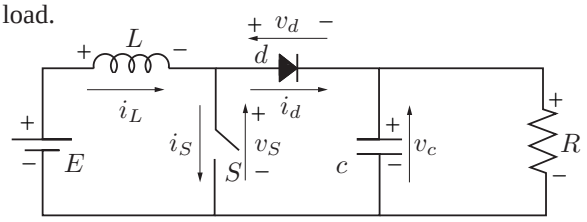

Fig. 1. Schematic representation of the DC-DC Boost converter.

The presence of switching elements (d and S) causes the overall system to be of a switching/hybrid nature. Depending on the (discrete) state of the diode and of the switch, one can distinguish four modes of operation [11]:

mode 1: $(S = 0, d = 1)$ mode 2: $(S = 1, d = 0)$
mode 3: $(S = 0, d = 0)$ mode 4: $(S = 1, d = 1)$

The circuits associated to each mode are shown in Figure 2. When the system is in mode 1, in which the switch is open ($S = 0$) and the diode is conducting ($d = 1$), the inductor is charged by the input source, which, also offloads power to the resistor. In mode 2, in which the switch is closed ($S = 1$) and the diode is blocking ($d = 0$), the inductor is charged by the input source and the capacitor is offloading its charge to the load. In mode 3, the capacitor offloads its charge to the load. Finally, mode 4, in which the switch is closed, the diode is conducting and the voltage in the capacitor is zero, hence only the inductor is charging. Using the ideal diode model:

$$\begin{aligned} &\text{conducting } (d = 1): && i_d \geq 0, v_d = 0 \\ &\text{blocking } (d = 0): && i_d = 0, v_d \leq 0 \end{aligned}$$

and the ideal switch model:

$$\begin{aligned} &\text{conducting } (S = 1): && v_S = 0 \\ &\text{blocking } (S = 0): && i_S = 0 \end{aligned}$$

the differential equations for each mode, along with the specific values of S and d, are given by

$$1: \begin{cases} S &= 0 \\ d &= 1 \\ \frac{d}{dt} v_c &= -\frac{1}{Rc} v_c + \frac{1}{c} i_L \\ \frac{d}{dt} i_L &= -\frac{1}{L} v_c + \frac{E}{L} \end{cases} \qquad 2: \begin{cases} S &= 1 \\ d &= 0 \\ \frac{d}{dt} v_c &= -\frac{1}{Rc} v_c \\ \frac{d}{dt} i_L &= \frac{E}{L} \end{cases}$$

$$3: \begin{cases} S &= 0 \\ d &= 0 \\ \frac{d}{dt} v_c &= -\frac{1}{Rc} v_c \\ \frac{d}{dt} i_L &= 0 \end{cases} \qquad 4: \begin{cases} S &= 1 \\ d &= 1 \\ \frac{d}{dt} v_c &= 0 \\ \frac{d}{dt} i_L &= \frac{E}{L} \end{cases}$$

In addition to the differential equations indicated above, the inequalities present in the ideal diode model impose further algebraic conditions on the states i_L and v_c for each individual mode. These mode-dependent conditions can be derived by inspecting for which states i_L and v_c a flow can take place in the mode over a time interval of positive length. This leads to the following conditions:

- For the diode to stay conducting while in mode 1, since $i_d = i_L$, we need
$$i_L > 0, \text{ or } (v_c \leq E, \, i_L = 0).$$
Note that the ideal diode model being used implies that during this mode we should have $v_d = 0$.
- For the diode to stay blocking during mode 2, since $v_d = -v_c$, we should have
$$v_c \geq 0.$$
Note that in this mode i_L is unconstrained.
- For the diode to be blocking during mode 3, we should have $v_d \leq 0$. Since for the configuration in mode 3, we have $v_d = E - v_c$, then this implies
$$v_c > E.$$
Moreover, since the diode is blocking and the switch is open, we shall have
$$i_L = 0.$$
- For the diode to stay conducting in mode 4 (which requires $v_d = 0$) since $v_d = -v_c$, we have
$$v_c = 0.$$
Since the diode is grounding the capacitor, no current can circulate through the diode, hence
$$i_d = 0.$$

Combining the conditions above with the differential equations for each mode, the resulting constrained algebraic differential equations for each mode are given in terms of (S, v_c, i_L) as follows:

$$1: \begin{cases} S &= 0 \\ \frac{d}{dt} v_c &= -\frac{1}{Rc} v_c + \frac{1}{c} i_L \\ \frac{d}{dt} i_L &= -\frac{1}{L} v_c + \frac{E}{L} \\ i_L &> 0, \text{ or } (v_c \leq E, \, i_L = 0) \end{cases} \qquad 2: \begin{cases} S &= 1 \\ \frac{d}{dt} v_c &= -\frac{1}{Rc} v_c \\ \frac{d}{dt} i_L &= \frac{E}{L} \\ v_c &\geq 0 \end{cases}$$

$$3: \begin{cases} S & = 0 \\ \frac{d}{dt}v_c & = -\frac{1}{Rc}v_c \\ \frac{d}{dt}i_L & = 0 \\ v_c & > E,\ i_L = 0 \end{cases} \qquad 4: \begin{cases} S & = 1 \\ \frac{d}{dt}v_c & = 0 \\ \frac{d}{dt}i_L & = \frac{E}{L} \\ v_c & = 0 \end{cases}$$

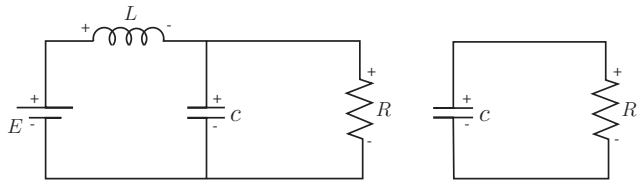

(a) mode 1 (b) mode 3

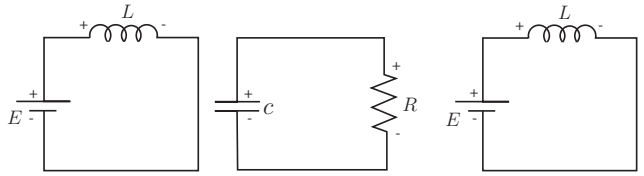

(c) mode 2 (d) mode 4

Fig. 2. Four different modes for the Boost converter.

From the above, it is clear that mode 2 and mode 4 can be combined into a single mode 2' with the following dynamics:

$$2': \begin{cases} S & = 1 \\ \frac{d}{dt}v_c & = -\frac{1}{Rc}v_c \\ \frac{d}{dt}i_L & = \frac{E}{L} \\ v_c & \geq 0,\ \text{any sign of } i_L \end{cases}$$

Therefore, the value of the switch S determines whether the system is in mode 1/mode 3 ($S = 0$, $i_L \geq 0$) or mode 2' ($S = 1$, $v_C \geq 0$). Note that it is possible that when S changes, v_c and i_L may not be in the regions of viability in the subsequent mode, in which case v_c and i_L should be appropriately reset. As a physical interpretation of a reset, one might think of an instantaneous discharge of the capacitor, which will happen if the capacitor is short-circuited. These resets can be formalized through consistency projectors mapping the state to the algebraic conditions of the subsequent mode [9], [10], [15], [16]. Although, a full model with resets can be derived, see [11], for practical operation of the converter it is clearly undesirable that such resets occur as they may damage the circuit. Therefore, to avoid such resets, our controller will allow $S = 0$ only when $i_L \geq 0$, and $S = 1$ only when $v_c \geq 0$. Indeed, in Section III-A, we propose a controller that guarantees that after every switch of S, the algebraic conditions of the subsequent mode are satisfied.

For convenience, we define $x := (v_c, i_L)$ and the algebraic constraints for the modes above in terms of sets as follows:

$$M_1 = \{x \in \mathbb{R}^2 \ : \ i_L > 0\} \cup \{x \in \mathbb{R}^2 \ : \ v_c \leq E,\ i_L = 0\},$$
$$M_{2'} = \{x \in \mathbb{R}^2 \ : \ v_c \geq 0\},$$
$$M_3 = \{x \in \mathbb{R}^2 \ : \ v_c > E,\ i_L = 0\}$$

Hence, $S = 0$ is only allowed when $x \in M_1 \cup M_3$ and $S = 1$ is only allowed when $x \in M_{2'}$. Using these restrictions, we can derive a switched differential inclusion encompassing all the modes of operation derived so far.

B. Mathematical model

In this section, we define a mathematical model of the Boost converter in which the differential equations in each mode define the continuous dynamics. Since the vector field associated with mode 1 is

$$f_a(x) = \begin{bmatrix} -\frac{1}{Rc}v_c + \frac{1}{c}i_L \\ -\frac{1}{L}v_c + \frac{E}{L} \end{bmatrix}$$

and the vector field associated with mode 3 is

$$f_b(x) = \begin{bmatrix} -\frac{1}{Rc}v_c \\ 0 \end{bmatrix}$$

the resulting vector field for $S = 0$ is discontinuous. To establish robust asymptotic stability of the upcoming closed-loop system, a Krasovskii regularization[1] of the vector field will be performed following the ideas in [17], [18]. The system will take the form of a switched differential inclusion with constraints, namely

$$\dot{x} \in F_S(x) \qquad x \in \widetilde{M}_S \tag{1}$$

where $S \in \{0, 1\}$ is the position of the switch S, and for each $S \in \{0, 1\}$, $F_S(x)$ is the Krasovskii regularization of the vector fields and $\widetilde{M}_S$ is the corresponding regularization of the sets capturing the regions of validity for each mode.

Following [18], the regularization of $\widetilde{M}_S$ for $S = 0$ is $\widetilde{M}_0 = \overline{M_1 \cup M_3} = \{x \in \mathbb{R}^2 : i_L \geq 0\}$, and $\widetilde{M}_S$ for $S = 1$ is $\widetilde{M}_1 = \overline{M_{2'}} = \{x \in \mathbb{R}^2 : v_c \geq 0\}$. Note that for $x \in \overline{M_3}$, f_a and f_b reduce to

$$f_a(x) = \begin{bmatrix} -\frac{1}{Rc}v_c \\ -\frac{1}{L}v_c + \frac{E}{L} \end{bmatrix}, \quad f_b(x) = \begin{bmatrix} -\frac{1}{Rc}v_c \\ 0 \end{bmatrix}.$$

Then, we have the discontinuous vector field for mode 1 and mode 3 as

$$f_0(x) = \begin{cases} f_a(x) & \text{if } x \in M_1; \\ f_b(x) & \text{if } x \in M_3. \end{cases}$$

The regularization of f_0 at each $x \in \widetilde{M}_0$ is given by

$$F_0(x) := \bigcap_{\delta > 0} \overline{\text{co}} f_0\left((x + \delta\mathbb{B}) \cap \widetilde{M}_0\right) \tag{2}$$

$$= \begin{cases} \{f_a(x)\} & \text{if } x \in \overline{M_1} \setminus \overline{M_3} \\ \overline{\text{co}}\left\{\begin{bmatrix} -\frac{1}{Rc}v_c \\ -\frac{1}{L}v_c + \frac{E}{L} \end{bmatrix}, \begin{bmatrix} -\frac{1}{Rc}v_c \\ 0 \end{bmatrix}\right\} & \text{if } x \in \overline{M_3} \end{cases}$$

$$= \begin{cases} \left\{\begin{bmatrix} -\frac{1}{Rc}v_c + \frac{1}{c}i_L \\ -\frac{1}{L}v_c + \frac{E}{L} \end{bmatrix}\right\} & \text{if } x \in \overline{M_1} \setminus \overline{M_3} \\ \{-\frac{1}{Rc}v_c\} \times \left[-\frac{1}{L}v_c + \frac{E}{L},\ 0\right] & \text{if } x \in \overline{M_3} \end{cases}$$

Since the vector field for mode 2' is given by $f_1(x) = \begin{bmatrix} -\frac{1}{Rc}v_c \\ \frac{E}{L} \end{bmatrix}$ which is continuous, we have for each $x \in \widetilde{M}_1$

$$F_1(x) = \{f_1(x)\} \tag{3}$$

The model (1) is a constrained switched differential inclusion. This is a key difference with previous modeling approaches (see, e.g. [6], [7]) where the third mode is omitted. Based on this complete model, we propose a controller that induces robust, global asymptotic stability of desired (output voltage) setpoints in the next section. As we will see, the hybrid systems approach proposed here is the enabling tool to achieve this result.

III. State-dependent switching law

In this section, a switching control law for the model (1) of the Boost converter is proposed. In Section IV, we will

[1]A Krasovskii regularization of this vector field is used due to the fact that the discontinuity occurs on a set of measure zero. A Filippov regularization would not account for discontinuities on such sets and would yield an incomplete mapping for mode 1 and mode 3. In fact, the Filippov regularization would yield a singleton set f_a on $\overline{M}_1$.

establish that this control law induces a robust and global asymptotic stability property. Besides that, we determine various robustness properties of the closed-loop system. To propose the control law, we will use a control Lyapunov function (CLF) approach, see [19].

A. Control Lyapunov function

Given a desired set-point voltage $v_c^* > 0$ and current $i_L^* > 0$, let $x^* = (v_c^*, i_L^*)$ and consider the CLF candidate

$$V(x) = (x - x^*)^\top P (x - x^*) \tag{4}$$

where $P = \begin{bmatrix} p_{11} & 0 \\ 0 & p_{22} \end{bmatrix} > 0$. To establish that the function V is indeed a CLF [19], we need to show that for each state $x = (v_c, i_L)$ of relevance there exists a choice of $S \in \{0, 1\}$ such that the derivative of V along (1) is negative. To do so, we compute the inner product between the gradient of V and the directions belonging to the (set-valued) map F_S in (1).

- For $S = 0$ and each $x \in \overline{M_1} \setminus \overline{M_3}$, we get

$$\begin{aligned}\langle \nabla V(x), F_0(x) \rangle &= \langle \nabla V(x), f_a(x) \rangle \\ &= 2p_{11}(v_c - v_c^*)\left(-\frac{1}{Rc}v_c + \frac{1}{c}i_L\right) + \\ &\qquad 2p_{22}(i_L - i_L^*)\left(\frac{-v_c + E}{L}\end{aligned} \tag{5}$$

- For $S = 0$ and each $x \in \overline{M_3}$, since $F_0(x)$ is a set, we have

$$\max_{\xi \in F_0(x)} \langle \nabla V(x), \xi \rangle =$$

$$\max_{\xi_1 = -\frac{1}{Rc}v_c,\ \xi_2 \in \left[-\frac{1}{L}v_c + \frac{E}{L},\ 0\right]} \langle [2p_{11}(v_c - v_c^*),\ \ 2p_{22}(i_L - i_L^*)]^\top, \xi \rangle =$$

$$2p_{11}(v_c - v_c^*)\left(-\frac{1}{Rc}v_c\right) + \max_{\xi_2 \in \left[-\frac{1}{L}v_c + \frac{E}{L},\ 0\right]} 2p_{22}(i_L - i_L^*)\xi_2 =$$

$$\begin{cases} 2p_{11}(v_c - v_c^*)\left(-\frac{1}{Rc}v_c\right) & \text{if} \quad i_L \geq i_L^* \\ 2p_{11}(v_c - v_c^*)\left(-\frac{1}{Rc}v_c\right) + & \\ \qquad 2p_{22}(i_L - i_L^*)\left(-\frac{1}{L}v_c + \frac{E}{L}\right) & \text{if} \quad i_L < i_L^* \end{cases}$$

Since $i_L^* > 0$ and every point in $\overline{M_3}$ is such that $i_L = 0$, inequality $i_L \geq i_L^*$ will never happen for points in $\overline{M_3}$. Then, for $S = 0$ and each $x \in \overline{M_3}$, we have

$$\begin{aligned}\max_{\xi \in F_0(x)} \langle \nabla V(x), \xi \rangle = 2p_{11}(v_c - v_c^*)\left(-\frac{1}{Rc}v_c\right) + \\ 2p_{22}(i_L - i_L^*)\left(-\frac{1}{L}v_c + \frac{E}{L}\right)\end{aligned} \tag{6}$$

- For $S = 1$ and each $x \in \overline{M_2}$, we get

$$\langle \nabla V(x), F_1(x) \rangle = \langle \nabla V(x), f_1(x) \rangle = 2p_{11}(v_c - v_c^*)\left(-\frac{1}{Rc}v_c\right) + 2p_{22}(i_L - i_L^*)\left(\frac{E}{L}\right) \tag{7}$$

Define for each $x \in \mathbb{R}^2$

$$\begin{aligned}\gamma_0(x) := 2p_{11}(v_c - v_c^*)\left(-\frac{1}{Rc}v_c + \frac{1}{c}i_L\right) + \\ 2p_{22}(i_L - i_L^*)\left(\frac{-v_c + E}{L}\right)\end{aligned} \tag{8}$$

$$\gamma_1(x) := 2p_{11}(v_c - v_c^*)\left(-\frac{1}{Rc}v_c\right) + 2p_{22}(i_L - i_L^*)\left(\frac{E}{L}\right) \tag{9}$$

Combining (5)-(7) and observing that the expressions in (5) and (6) are equal, for each $S \in \{0, 1\}$ and $x \in \widetilde{M}_S$ we get

$$\max_{\xi \in F_S(x)} \langle \nabla V(x), \xi \rangle = \begin{cases} \gamma_0(x) & \text{if} \quad S = 0 \\ \gamma_1(x) & \text{if} \quad S = 1 \end{cases} \tag{10}$$

The sign of the functions γ_0, γ_1 will be used to define a state-dependent switching control law assigning the control input S. Let

$$\mathcal{A}_x = \{x \in \mathbb{R}^2 \ : \ v_c = v_c^*,\ i_L = i_L^*\} \tag{11}$$

define the isolated point to be stabilized, namely, the point $(v_c, i_L) = x^* = (v_c^*, i_L^*)$. The following lemma establishes a property of the functions γ_0, γ_1 that will be instrumental in our stability result in Section IV-A and, in fact, shows that V is a CLF [19] for (1). The constraints $\widetilde{M}_S$ on the switching are not taken into account at this point, but are incorporated again later (see Proposition IV.2 below).

Lemma III.1. *Let $R, E, p_{11}, p_{22} > 0$, $\frac{p_{11}}{c} = \frac{p_{22}}{L}$, $v_c^* > E$, and $i_L^* = \frac{v_c^{*2}}{RE}$. Then, for each $x \in \mathbb{R}^2 \setminus \mathcal{A}_x$, there exists $S \in \{0, 1\}$ such that*

$$\gamma_S(x) < 0 \tag{12}$$

Moreover, $\{x \in \mathbb{R}^2 \ : \ \gamma_S(x) = 0,\ S \in \{0, 1\}\} = \mathcal{A}_x$.

Proof. Consider the functions γ_S, $S \in \{0, 1\}$, using the relationship $\frac{p_{11}}{c} = \frac{p_{22}}{L}$, we can rewrite (8) and (9) as

$$\gamma_0(x) = 2(A_0 v_c^2 + B_0 v_c + C_0 i_L + D_0) \tag{13}$$

$$\gamma_1(x) = 2(A_1 v_c^2 + B_1 v_c + C_1 i_L + D_1) \tag{14}$$

where the coefficients, A_0 through D_0 and A_1 through D_1 are defined as

$$\begin{aligned} A_0 &= -\frac{p_{11}}{Rc} & A_1 &= -\frac{p_{11}}{Rc} \\ B_0 &= \frac{p_{11}v_c^*}{Rc} + \frac{p_{22}i_L^*}{L} & B_1 &= \frac{p_{11}v_c^*}{Rc} \\ C_0 &= -\frac{p_{11}v_c^*}{c} + \frac{p_{22}E}{L} & C_1 &= \frac{p_{22}E}{L} \\ D_0 &= -\frac{p_{22}i_L^*E}{L} & D_1 &= -\frac{p_{22}i_L^*E}{L} \end{aligned}$$

To guarantee that for every $(v_c, i_L) \in \mathbb{R}^2 \setminus \mathcal{A}_x$ there exists an $S \in \{0, 1\}$ such that $\gamma_S(x) < 0$ and that $\{x \in \mathbb{R}^2 \ : \ \gamma_S(x) = 0,\ S \in \{0, 1\}\} = \mathcal{A}_x$, we consider the sets $\Gamma_S := \{x \in \mathbb{R}^2 \ : \ \gamma_S(x) < 0\}$ for $S \in \{0, 1\}$. We will also use the boundaries of the sets Γ_S given by $\Omega_S := \{x \in \mathbb{R}^2 \ : \ \gamma_S(x) = 0\}$ for $S \in \{0, 1\}$, which are parabolas. We first derive explicit expressions for Γ_S, $S \in \{0, 1\}$, next.

(i) For $x \in \Gamma_0$, we have $A_0 v_c^2 + B_0 v_c + C_0 i_L + D_0 < 0$. Substituting the coefficients A_0 through D_0, using $\frac{p_{11}}{c} = \frac{p_{22}}{L}$ and $v_c^* > E$ gives

$$i_L > \frac{1}{E - v_c^*}\left(\frac{1}{R}v_c^2 - \left(\frac{v_c^*}{R} + i_L^*\right)v_c + i_L^* E\right) \tag{15}$$

(ii) For $x \in \Gamma_1$, we have $A_1 v_c^2 + B_1 v_c + C_1 i_L + D_1 < 0$. Substituting the coefficients A_1 through D_1, using again $\frac{p_{11}}{c} = \frac{p_{22}}{L}$ gives

$$i_L < \frac{1}{RE}v_c^2 - \frac{v_c^*}{RE}v_c + i_L^* \tag{16}$$

This gives the expressions

$$\begin{aligned}\Gamma_0 = \Bigg\{(v_c, i_L) \in \mathbb{R}^2 \ : \ i_L > \\ \frac{1}{E - v_c^*}\left(\frac{1}{R}v_c^2 - \left(\frac{v_c^*}{R} + i_L^*\right)v_c + i_L^* E\right)\Bigg\}\end{aligned} \tag{17}$$

$$\Gamma_1 = \left\{(v_c, i_L) \in \mathbb{R}^2 \ : \ i_L < \frac{1}{RE}v_c^2 - \frac{v_c^*}{RE}v_c + i_L^*\right\} \tag{18}$$

and similar ones for Ω_S, $S \in \{0, 1\}$. Both parabolas Ω_S,

$S \in \{0,1\}$, have their axis of symmetry parallel to the i_L-axis. Hence, we have to show now that $\Gamma_1 \cup \Gamma_2 = \mathbb{R}^2 \setminus \mathcal{A}_x$ and $\Omega_0 \cap \Omega_1 = \mathcal{A}_x$.

To shows this, note that $\frac{1}{(E-v_c^*)} < 0$ indicating that Ω_0 is a "downward" parabola (it has a maximum in i_L-direction) and Γ_0 is the region above it. Similarly, since $\frac{1}{RE} > 0$, Ω_1 is an "upward" parabola (it has a minimum in i_L-direction) and Γ_1 is the region below it. See Figure 3 for an illustration. If we now can show that $\Omega_0 \cap \Omega_1 = \mathcal{A}_x$, then it follows that $\Gamma_1 \cup \Gamma_2 = \mathbb{R}^2 \setminus \mathcal{A}_x$ as in Figure 3, and the proof of the lemma is complete.

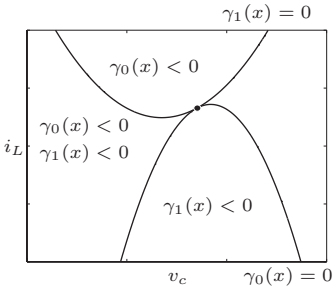

Fig. 3. An example of a possible sign distribution for the two parabolas $\gamma_0(x) = 0$ and $\gamma_1(x) = 0$.

To show that $\Omega_0 \cap \Omega_1 = \mathcal{A}_x$, we observe that if $(v_c, i_L) \in \Omega_0 \cap \Omega_1$ we must have that the right-hand sides of (16) and (15) are equal, which leads to

$$\left(-\frac{1}{R}v_c^2 + \left(\frac{v_c^*}{R} + i_L^*\right)v_c - i_L^* E\right)\frac{1}{E - v_c^*} = -\frac{1}{RE}v_c^2 + \frac{v_c^*}{RE}v_c - i_L^*. \tag{19}$$

Since $i_L^* = \frac{v_c^{*2}}{RE}$, we have

$$-\frac{v_c^*}{RE}(v_c^2 - 2v_c^* v_c + (v_c^*)^2) = 0,$$

which has a unique solution $v_c = v_c^*$, and implies that $\Omega_0 \cap \Omega_1$ is indeed $\{(v_c^*, i_L^*)\}$. This completes the proof. □

The property in Lemma III.1 shows indeed that V is a CLF-like function in the sense that

$$\min_{S\in\{0,1\}} \max_{\xi \in F_S(x)} \langle \nabla V(x), \xi \rangle < 0 \qquad \forall x \in \mathbb{R}^2 \setminus \mathcal{A}_x \tag{20}$$

This condition can be used to derive a suitable stabilizing control law, as will be done next.

B. Proposed control law

The condition obtained in (20) naturally leads to the following selection of the input S, which is a nonlinear system with discontinuous right-hand side (if we forget for a moment the constraints on the switching in (1)):

$$S = \arg\min_{S'\in\{0,1\}} \max_{\xi \in F_{S'}(x)} \langle \nabla V(x), \xi \rangle \tag{21}$$

The control law, which we will propose below, will take advantage of this observation. However, the direct application of (21) as the switching law, leads to a discontinuous control law and results in chattering (sliding motions; see [7]), which is undesirable in practice. Therefore, we will propose a modified logic-based control law (and a corresponding regularized closed-loop system), which is practically feasible. In fact, for the resulting (regularized) controller various robustness properties can be derived and proved mathematically based on the hybrid system setup particularly chosen for this purpose (see Section IV below).

Let $q \in \{0,1\}$ be a logic state indicating the value of the actual input S. The envisioned logic-based control law will select the input according to the current active input q and the value of the state, namely, when certain well-designed functions $\widetilde{\gamma}_q$ become zero. These functions $\widetilde{\gamma}_q$ are control design parameters that are related to the functions γ_q in (13) and (14) and will be chosen as in the following lemma.

Remark III.2. *The functions $\widetilde{\gamma}_q$ are not chosen exactly equal to γ_q, because mode 1 would have an equilibrium $(v_c, i_L) = \left(E, \frac{E}{R}\right)$ exactly at $\gamma_0(x) = 0$. This would prevent to achieve global asymptotic stability of the desired setpoint.*

Lemma III.3. *Let $R, E, p_{11}, p_{22} > 0$, $\frac{p_{11}}{c} = \frac{p_{22}}{L}$, $v_c^* > E$, and $i_L^* = \frac{v_c^{*2}}{RE}$. For each $q \in \{0,1\}$, let $\widetilde{\gamma}_q$ be given for $x \in \mathbb{R}^2$ as*

$$\widetilde{\gamma}_0(x) = \gamma_0(x) + K_0 (v_c - v_c^*)^2 \tag{22}$$

$$\widetilde{\gamma}_1(x) = \gamma_1(x) + K_1 (v_c - v_c^*)^2 \tag{23}$$

and $K_0 \in \left(0, \frac{2p_{11}}{Rc}\right)$, $K_1 \in \left(0, \frac{2p_{11}}{Rc}\right)$. The following hold:

(a) For $q \in \{0,1\}$ and $x \notin \mathcal{A}_x$ we have that $\widetilde{\gamma}_q(x) \geq 0$ implies $\widetilde{\gamma}_{1-q}(x) < 0$;

(b) For $q \in \{0,1\}$ and $x \notin \mathcal{A}_x$ we have that $\widetilde{\gamma}_q(x) \leq 0$ implies $\gamma_q(x) < 0$;

(c) For $x \in \mathbb{R}^2$ it holds that
$\frac{1}{C_0}\lim_{K_0 \to \frac{2p_{11}}{Rc}} \widetilde{\gamma}_0(x) = \frac{1}{C_1}\lim_{K_1 \to \frac{2p_{11}}{Rc}} \widetilde{\gamma}_1(x) = -\frac{2i_L^*}{v_c^*}v_c + 2i_L$,
$\lim_{K_0 \to 0} \widetilde{\gamma}_0(x) = \gamma_0(x)$, $\lim_{K_1 \to 0} \widetilde{\gamma}_1(x) = \gamma_1(x)$.

The proof is given in Appendix A.

Based on the properties derived in the lemma above we can define an appropriate (robustly) stabilizing control law. In fact, the control law makes sure that for the current value of q and x it holds that $\widetilde{\gamma}_q(x) \leq 0$, which implies by property *(b)* that as long as $x \notin \mathcal{A}_x$, we have that $\gamma_q(x) < 0$, which, in turn, implies that the CLF V in (4) is decreasing. Once $\widetilde{\gamma}_q(x)$ becomes 0, a switch occurs from q to $1-q$, and, due to property *(a)* in the above lemma, we have then that $\widetilde{\gamma}_{1-q}(x) < 0$ if $x \notin \mathcal{A}_x$, and hence, the switching is well defined. The constants K_0 and K_1 control the shape and position of the switching boundaries, which are parabolas in the (v_c, i_L) plane. In fact, according to property *(c)* of Lemma III.3, as K_0 and K_1 approach zero, the switching boundary approaches the zero level set of $\gamma_0(x)$ and γ_1, respectively. Moreover, as K_0 and K_1 approach $\frac{2p_{11}}{Rc}$, the switching boundaries approach the line given by the points x such that $-\frac{2i_L^*}{v_c^*}v_c + 2i_L = 0$.

S is assigned to q, namely, $S = q$, and combining this with the constraints in (1), leads to the hybrid system $\mathcal{H}$ given by

$$\begin{aligned} \begin{bmatrix} \dot{x} \\ \dot{q} \end{bmatrix} &\in \begin{bmatrix} F_q(x) \\ 0 \end{bmatrix} =: F(x,q) \qquad (x,q) \in C \\ \begin{bmatrix} x^+ \\ q^+ \end{bmatrix} &= \begin{bmatrix} x \\ G_q(x) \end{bmatrix} =: G(x,q) \qquad (x,q) \in D \end{aligned} \tag{24}$$

where

$$C = \left\{(x,q) : x \in \widetilde{M}_0,\ \widetilde{\gamma}_0(x) \leq 0,\ q = 0\right\} \cup \left\{(x,q) : x \in \widetilde{M}_1,\ \widetilde{\gamma}_1(x) \leq 0,\ q = 1\right\}$$

$$D = \left\{(x,q) : x \in \widetilde{M}_0,\ \widetilde{\gamma}_0(x) = 0,\ q = 0\right\} \cup \left\{(x,q) : x \in \widetilde{M}_1,\ \widetilde{\gamma}_1(x) = 0\ q = 1\right\}$$

and, for each $(x,q) \in \mathbb{R}^3$, G_q is continuous and at points $(x,q) \in \mathbb{R}^2 \times \{0,1\}$ is given by

$$G_q(x) = \begin{cases} \{1\} & \text{if} \quad q = 0 \\ \{0\} & \text{if} \quad q = 1 \end{cases}$$

The flow map F of the hybrid system $\mathcal{H}$ is constructed by stacking the map F_S (with $S = q$) of (1) and zero, while the flow set enforces the constraints in (1) as well as those of the switching mechanism of the proposed controller. In this way, the continuous evolution of x is according to (1) under the effect of the proposed controller, while q does not change during flows. The jump map G is such that x does not change at jumps and q is toggled at jumps, while the jump set enforces the jumps of $G_q(x)$ within the constraints of (1), as we will prove below (see Proposition IV.2).

Sample contour plots and switching boundaries $\gamma_q(x) = 0$ and $\widetilde{\gamma}_q(x) = 0$ of the proposed controller for a particular set of parameters ($x^* = (7,\ 3.27)$, $E = 5$V, $R = 3\Omega$, $c = 0.1$F, $L = 0.2$H, $p_{11} = \frac{c}{2}$, $p_{22} = \frac{L}{2}$, and varying K_0 and K_1) are shown in Figure 4. By varying the constants $K_0 \in$

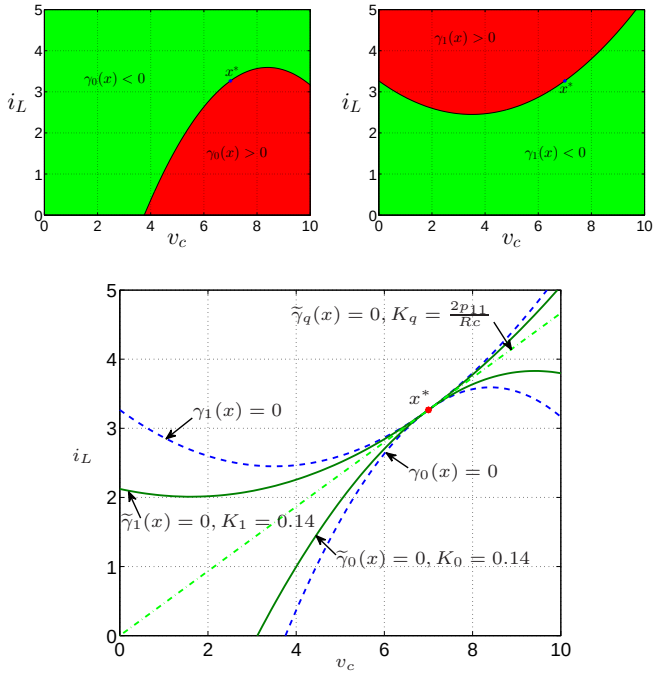

Fig. 4. The switching boundaries $\gamma_q(x) = 0$ and $\widetilde{\gamma}_q(x) = 0$, when $x^* = (7, 3.27)$, $E = 5$V, $R = 3\Omega$, $c = 0.1$F, $L = 0.2$H, $p_{11} = \frac{c}{2}$, $p_{22} = \frac{L}{2}$, and different values for K_0 and K_1.

$(0, \frac{2p_{11}}{Rc})$ and $K_1 \in (0, \frac{2p_{11}}{Rc})$, the shape and the position of the switching boundaries can be controlled. Some examples are shown in Figure 4. Note that the switching boundaries can also be modified by changing system parameters R and E (because of uncertainties in supply and demand of renewable energy sources).

In the next section we derive important properties of the resulting closed-loop system $\mathcal{H}$.

IV. Stability and Robustness Properties

To prove closed-loop properties of the hybrid system $\mathcal{H}$ regarding stability and robustness, we first recall some preliminaries.

A. Preliminaries on hybrid systems

Depending on the flow and the jump dynamics, solutions to the closed-loop system $\mathcal{H}$ evolve either continuously or discretely. Following [20], we treat the number of jumps as an independent variable j next to the usual time and we parameterize the hybrid time by (t,j). Solutions to $\mathcal{H}$ will be given on hybrid time domains, which are defined next.

First, a set $S \subset \mathbb{R}_{\geq 0} \times \mathbb{N}$ is a compact hybrid time domain if

$$S = \bigcup_{j=0}^{J-1} ([t_j, t_{j+1}], j)$$

for some finite sequence of times $0 = t_0 \leq t_1 \leq t_2 \cdots \leq t_J$. A set $S \subset \mathbb{R}_{\geq 0} \times \mathbb{N}$ is a hybrid time domain if for all $(T,J) \in S$, $S \cap ([0,T] \times \{0,1,\ldots J\})$ is a compact hybrid time domain. A hybrid arc, as defined in [14], is a function x defined on $\operatorname{dom} x$ that is locally absolutely continuous in t on $\operatorname{dom} x \cap (\mathbb{R}_{\geq 0} \times \{j\})$ for each $j \in \mathbb{N}$. For hybrid arcs x, we will use the following definitions regarding its domain:

- $\sup_t \operatorname{dom}\ x = \sup\{t \in \mathbb{R}_{\geq 0} : \exists j \in \mathbb{N}$ such that $(t,j) \in \operatorname{dom}\ x\}$
- $\sup_j \operatorname{dom}\ x = \sup\{j \in \mathbb{N} : \exists t \in \mathbb{R}_{\geq 0}$ such that $(t,j) \in \operatorname{dom}\ x\}$
- $\sup \operatorname{dom}\ x = \left(\sup_t \operatorname{dom}\ x, \sup_j \operatorname{dom}\ x\right)$

Then, solutions (or trajectories) to the general hybrid system

$$\begin{aligned} \dot{\xi} &\in F(\xi), \qquad \xi \in C \\ \xi^+ &= G(\xi), \qquad \xi \in D \end{aligned} \tag{25}$$

with state $\xi \in \mathbb{R}^n$ are defined as follows: a hybrid arc $\chi : \operatorname{dom} \chi \to \mathbb{R}^n$ is a solution to the hybrid system (25) if $\chi(0,0) \in C \cup D$ and

(S1) For all $j \in \mathbb{N}$,

$$\begin{aligned} &\chi(t,j) \in C && \text{for all } t \\ &\dot{\chi}(t,j) \in F(\chi(t,j)) && \text{for almost all } t \end{aligned}$$

such that $(t,j) \in \operatorname{dom} \chi$.

(S2) For all $(t,j) \in \operatorname{dom} x$ such that $(t,j+1) \in \operatorname{dom} x$,

$$\chi(t,j) \in D, \qquad \chi(t,j+1) = G(\chi(t,j))$$

A solution χ is said to be maximal if there does not exist a solution χ' such that χ is a truncation of χ' to some proper subset of $\operatorname{dom} \chi'$. A solution is called nontrivial if $\operatorname{dom} \chi$ contains at least one point different from $(0,0)$. A solution is said to be complete if $\operatorname{dom} \chi$ is unbounded.

We will use [14, Proposition 6.10] to prove the existence and completeness of solutions to the proposed system. For self-containedness, we recall [14, Proposition 6.10] next.

Proposition IV.1. *Let $\mathcal{H} = (C, F, D, G)$ satisfy the hybrid basic conditions, i.e., its data (C, F, D, G) is such that*[2]

(A1) C and D are closed sets;

(A2) $F : \mathbb{R}^3 \rightrightarrows \mathbb{R}^3$ is outer semicontinuous and locally bounded relative to C, $C \subset \operatorname{dom} F$, and $F(x)$ is nonempty and convex for all $x \in C$;

(A3) $G : \mathbb{R}^3 \to \mathbb{R}^3$ is continuous and $D \subset \operatorname{dom} G$.

[2]A set-valued map $S : \mathbb{R}^n \rightrightarrows \mathbb{R}^m$ is *outer semicontinuous* at $x \in \mathbb{R}^n$ if for each sequence $\{x_i\}_{i=1}^{\infty}$ converging to a point $x \in \mathbb{R}^n$ and each sequence $y_i \in S(x_i)$ converging to a point y, it holds that $y \in S(x)$; see [21, Definition 5.4]. Given a set $X \subset \mathbb{R}^n$, it is *outer semicontinuous relative to X* if the set-valued mapping from $\mathbb{R}^n$ to $\mathbb{R}^m$ defined by $S(x)$ for $x \in X$ and $\emptyset$ for $x \notin X$ is outer semicontinuous at each $x \in X$. It is *locally bounded* if, for each compact set $K \subset \mathbb{R}^n$ there exists a compact set $K' \subset \mathbb{R}^n$ such that $S(K) := \cup_{x \in K} S(x) \subset K'$.

Take an arbitrary $\xi \in C \cup D$. If $\xi \in D$, or

(VC) there exists a neighborhood U of ξ such that for every $x \in U \cap C$,

$$F(x) \cap T_C(x) \neq \emptyset$$

then there exists a nontrivial solution ϕ to $\mathcal{H}$ with $\phi(0,0) = \xi$. If (VC) holds for every $\xi \in C \setminus D$, then there exists a nontrivial solution to $\mathcal{H}$ from every initial point in $C \cup D$, and every $\phi \in \mathcal{S}_{\mathcal{H}}$, where $\mathcal{S}_{\mathcal{H}}$ denotes the set of solutions of the hybrid system $\mathcal{H}$, satisfies exactly one of the following conditions:

(a) ϕ is complete;

(b) $\operatorname{dom}\phi$ is bounded and the interval I^J, where $J = \sup_j \operatorname{dom}\phi$, has nonempty interior and $t \mapsto \phi(t, J)$ is a maximal solution to $\dot{z} \in F(z)$, in fact $\lim_{t \to T} |\phi(t, J)| = \infty$, where $T = \sup_t \operatorname{dom}\phi$ (finite escape time);

(c) $\operatorname{dom}\phi(T, J) \notin C \cup D$, where $(T, J) = \sup \operatorname{dom}\phi$.

Furthermore, if $G(D) \subset C \cup D$, then (c) above does not occur.

The following result establishes that every solution to the closed-loop system is complete.

B. Completeness of trajectories

Proposition IV.2. *(Properties of solutions) For each $\xi \in C \cup D$, every maximal solution $\chi = (x, q)$ to the hybrid system $\mathcal{H} = (C, F, D, G)$ in* (24) *with $\chi(0,0) = \xi$ is complete.*

The proof is given in Appendix B.

C. Closed-loop stability

Our goal is to show that the compact set $\mathcal{A}$ in (11) is asymptotically stable. To this end, we employ the following stability notion for general hybrid systems [14].

Definition IV.3 (Stability)**.** *A compact set $\mathcal{A} \subset \mathbb{R}^n$ is said to be*

- stable *if for each $\varepsilon > 0$ there exists $\delta > 0$ such that each solution χ with $|\chi(0,0)|_{\mathcal{A}} \leq \delta$ satisfies $|\chi(t,j)|_{\mathcal{A}} \leq \varepsilon$ for all $(t,j) \in \operatorname{dom}\chi$;*
- attractive *if there exists $\mu > 0$ such that every maximal solution χ with $|\chi(0,0)|_{\mathcal{A}} \leq \mu$ is complete and satisfies $\lim_{(t,j) \in \operatorname{dom}\chi, t+j \to \infty} |\chi(t,j)|_{\mathcal{A}} = 0$;*
- asymptotically stable *if $\mathcal{A}$ is stable and attractive;*
- globally asymptotically stable *if the attractivity property holds for every point in $C \cup D$.*

The following result on the structural properties of $\mathcal{H}$ in (24) is key for robust stability, see [14].

Lemma IV.4. *The closed-loop system $\mathcal{H}$ given by* (24) *satisfies the hybrid basic conditions given by (A1)-(A3) in [14, Proposition 6.5].*

Proof. (A1) follows from the continuity of $\widetilde{\gamma}_S$ for each $S \in \{0,1\}$ and the closedness of $\widetilde{M}_0$ and $\widetilde{M}_1$. Next, (A2) follows from the Krasovskii regularization. Lastly, (A3) follows from the fact that the jump map is continuous. □

Using these properties, we are now ready to establish the following theorem, which states global asymptotic stability of the compact set $\mathcal{A}$ for the hybrid system $\mathcal{H}$.

Theorem IV.5. *Consider the hybrid system $\mathcal{H}$ in* (24) *with $c, L, R, E, K_0, K_1 > 0$. Given a desired set-point voltage and current (v_c^*, i_L^*), where $v_c^* > E$ and $i_L^* = \frac{v_c^{*2}}{RE}$, then the compact set*

$$\mathcal{A} = \mathcal{A}_x \times \{0,1\} \tag{26}$$

is globally asymptotically stable for $\mathcal{H}$.

Proof. Consider the function V given in (4) and define $\widetilde{V}(x,q) = V(x)$ for all $(x,q) \in C \cup D$. Note that $\widetilde{V}(x,q) = 0$ when $x \in \mathcal{A}_x$ and $\widetilde{V}(x,q) > 0$ for all $(x,q) \in (\mathbb{R}^2 \times \{0,1\}) \setminus \mathcal{A}_x$. From the computation of the inner product between ∇V and the direction belonging to F_S in (10), for each $(x,q) \in C$ (see Lemma III.1), we have

$$u_c(x,q) := \max_{\xi \in F(x,q)} \langle \nabla \widetilde{V}(x,q), \xi \rangle$$

$$= \begin{cases} (v_c - v_c^*)(-\frac{1}{R}v_c + i_L) + (i_L - i_L^*)(-v_c + E) = \\ \qquad \gamma_0(x) \leq 0 \text{ if } q = 0, \\ (v_c - v_c^*)\left(-\frac{1}{R}v_c\right) + (i_L - i_L^*)E = \\ \qquad \gamma_1(x) \leq 0 \text{ if } q = 1 \end{cases}$$

and, for each $(x,q) \in D$, we have

$$u_d(x,q) := \max_{\xi \in G(x,q)} \widetilde{V}(\xi) - \widetilde{V}(x,q) = 0 \tag{27}$$

Then, by [14, Theorem 3.18], the set (26) is stable.

To show attractivity, we apply the invariance principle in [22, Theorem 4.7]. To this end, we compute the zero level set of u_c and u_d defined above. It follows that

$$u_c^{-1}(0) = \{(x,q) \in C \ : \ u_c(x,q) = 0 \ \} = D$$
$$u_d^{-1}(0) = \{(x,q) \in D \ : \ u_d(x,q) = 0 \ \} = D$$

Then, each complete and bounded solution (x,q) to $\mathcal{H}$ converges to the largest weakly invariant[3] subset of the set

$$\left\{(x,q) \in C \cup D \ : \ \widetilde{V}(x,q) = r \ \right\} \cap \left(u_c^{-1}(0) \cup (u_d^{-1}(0) \cap G(u_d^{-1}(0)))\right) \tag{28}$$

for some $r \geq 0$. With the definitions above, the set of points (28) reduces to

$$\{(x,q) \in C \cup D \ : \ V(x) = r \ \} \cap D \tag{29}$$

Note that the only invariant set for $\mathcal{H}$ within (29) is $\mathcal{A}$ since solutions cannot stay in (29) unless $v_c = v_c^*$ and $i_L = i_L^*$ (i.e., $r = 0$). In fact, solutions to the hybrid systems $\mathcal{H}$ in (24) cannot stay in a constant level set of V since the equilibrium points of the vector field F do not belong to $C \cap D$ and, for points in $C \setminus D$, the derivative of V is negative for each $q \in \{0,1\}$. □

D. Robustness to general perturbations

The construction of the controller in Section III-A is such that the closed-loop system $\mathcal{H}$ has data satisfying the properties in Lemma IV.4. With these properties, we have that the asymptotic stability property asserted by Theorem IV.5 is robust to small perturbations. We consider the following model of the (regularized) plant in (1) with perturbations:

$$\dot{x} \in F_q(x + d_1) + d_2 \tag{30}$$

[3]For the set of hybrid trajectories $\mathcal{S}$, the set $\mathcal{M} \subset \mathcal{O}$ is said to be *weakly invariant* (with respect to $\mathcal{S}$) if it is both weakly forward invariant and weakly backward invariant; see [22, Definition 3.1], it is *weakly forward invariant* (with respect to $\mathcal{S}$) if for each $x^0 \in \mathcal{M}$, there exists at least one complete hybrid trajectory $x \in \mathcal{S}(x^0)$ with $x(t,j) \in \mathcal{M}$ for all $(t,j) \in \operatorname{dom} x$. It is *weakly backward invariant* (with respect to $\mathcal{S}$) if for each $q \in \mathcal{M}$, $N > 0$, there exist $x^0 \in \mathcal{M}$ and at least one hybrid trajectory $x \in \mathcal{S}(x^0)$ such that some $(t^*, j^*) = q$ and $x(t,j) \in \mathcal{M}$ for all $(t,j) \leq (t^*, j^*)$, $(t,j) \in \operatorname{dom} x$.

where d_1 corresponds to state noise and d_2 captures unmodeled dynamics. Then, defining $\widetilde{d}_i = (d_i, 0)$, the closed-loop system $\mathcal{H}$ results in the perturbed hybrid system, which is denoted by $\widetilde{\mathcal{H}}$, with state $\chi := (x, q)$ and dynamics

$$\begin{array}{rcll} \dot{\chi} & \in & F(\chi + \widetilde{d}_1) + \widetilde{d}_2 & \chi + \widetilde{d}_1 \in \widetilde{C} \\ \chi^+ & \in & G(\chi) & \chi + \widetilde{d}_1 \in \widetilde{D} \end{array}$$

The following result establishes a nominal robustness property of $\mathcal{H}$.

Theorem IV.6. *Under the assumptions of Theorem IV.5, there exists $\widetilde{\beta} \in \mathcal{KL}$ such that, for each $\widetilde{\varepsilon} > 0$ and each compact set $K \subset \mathbb{R}^2$, there exists $\delta > 0$ such that for any two measurable functions $\widetilde{d}_1, \widetilde{d}_2 : \mathbb{R}_{\geq 0} \to \delta\mathbb{B}$, every solution $\widetilde{\chi} = (\widetilde{x}, \widetilde{q})$ to $\widetilde{\mathcal{H}}$ with $\widetilde{\chi}(0,0) \in K \times \{0,1\}$ is such that its $\widetilde{x}$ component, namely, (v_c, i_L), satisfies*

$$|\widetilde{x}(t,j)|_{\mathcal{A}_x} \leq \widetilde{\beta}(|\widetilde{x}(0,0)|_{\mathcal{A}_x}, t+j) + \widetilde{\varepsilon} \quad \forall (t,j) \in \operatorname{dom} \widetilde{\chi} \tag{31}$$

Proof. Since $\mathcal{A}$ is asymptotically stable for $\mathcal{H}$, by [23, Theorem 6.5], there exists $\beta \in \mathcal{KL}$ such that all solutions χ to $\mathcal{H}$ satisfy $|\chi(t,j)|_{\mathcal{A}\times\{0,1\}} \leq \beta(|\chi(0,0)|_{\mathcal{A}\times\{0,1\}}, t+j)$ for all $(t,j) \in \operatorname{dom}\chi$. Consider the perturbed hybrid system $\widetilde{\mathcal{H}}$. Since $\widetilde{d}_1(t), \widetilde{d}_2(t) \in \delta\mathbb{B}$ for all $t \geq 0$, the closed-loop system $\widetilde{\mathcal{H}}$ can be written as

$$\begin{array}{ll} \dot{\chi} & \in F_\delta(\chi) \quad \chi \in C_\delta \\ \chi^+ & \in G_\delta(\chi) \quad \chi \in D_\delta \end{array} \tag{32}$$

where

$$\begin{aligned} F_\delta(\chi) &:= \overline{\text{co}} F(\chi + \delta\mathbb{B}) + \delta\mathbb{B}, \\ G_\delta(\chi) &:= \{\eta \ : \ \eta \in \chi' + \delta\mathbb{B}, \chi' \in G(\chi + \delta\mathbb{B}) \ \}, \\ C_\delta &:= \left\{\chi \ : \ (\chi + \delta\mathbb{B}) \cap \widetilde{C} \neq \emptyset \right\}, \\ D_\delta &:= \left\{\chi \ : \ (\chi + \delta\mathbb{B}) \cap \widetilde{D} \neq \emptyset \right\}. \end{aligned}$$

This hybrid system corresponds to an outer perturbation of $\mathcal{H}$ and satisfies (C1), (C2), (C3), and (C4) in [23] (see Example 5.3 in [23] for more details). Then, the claim follows by Theorem 6.6 in [23] since, for each compact set K of the state space and each $\widetilde{\varepsilon} > 0$, there exists $\delta^* > 0$ such that for each $\delta \in (0, \delta^*]$, every solution $\widetilde{\chi}$ to $\widetilde{\mathcal{H}}$ from K satisfies, for all $(t,j) \in \operatorname{dom}\widetilde{\chi}$, $|\widetilde{\chi}(t,j)|_{\mathcal{A}} \leq \beta(|\widetilde{\chi}(0,0)|_{\mathcal{A}}, t+j) + \widetilde{\varepsilon}$. This establishes the result since $|\widetilde{\chi}|_{\mathcal{A}_x\times\{0,1\}} = |\widetilde{x}|_{\mathcal{A}_x}$. □

Unlike previous results in the literature, this robustness property implies that our controller is robust to small measurement noise and unmodeled dynamics. In addition to the robustness to general perturbations shown above, the asymptotic stability of $\mathcal{A}$ is robust to slow variations of the system parameters, such as input voltage E and load R. Such a result follows from a direct application of [14, Corollary 7.27].

E. Robustness to spatial regularization

When the system reaches its desired steady state using the controller in Section IV-A, arbitrarily fast switching may occur. To alleviate this problem, spatial regularization is performed to the closed-loop system $\mathcal{H}$ (at the controller level). More precisely, γ_0 and γ_1 are modified by using a constant factor ρ, with $\rho \in \mathbb{R}_{\geq 0}$. The regularized system will be denoted as $\mathcal{H}^\rho$, and its flow map is given by the same equation as $\mathcal{H}$, i.e.,

$$\begin{bmatrix} \dot{x} \\ \dot{q} \end{bmatrix} \in \begin{bmatrix} F_q(x) \\ 0 \end{bmatrix} \qquad (x,q) \in C_\rho$$

where, now, the flow set is replaced by

$$\begin{aligned} C_\rho = &\left\{(x,q) : x \in \widetilde{M}_0, \ \widetilde{\gamma}_0(x) \leq \rho, \ q = 0\right\} \cup \\ &\left\{(x,q) : x \in \widetilde{M}_1, \ \widetilde{\gamma}_1(x) \leq \rho, \ q = 1\right\} \end{aligned}$$

Furthermore, the jump map is given by

$$\begin{array}{rcll} x^+ & = & x & \\ q^+ & \in & G_q(x) & (x,q) \in D_\rho \end{array}$$

where, now, the jump set is given by

$$\begin{aligned} D_\rho = &\left\{(x,q) : x \in \widetilde{M}_0, \ \ \widetilde{\gamma}_0(x) = \rho, \ q = 0\right\} \cup \\ &\left\{(x,q) : x \in \widetilde{M}_1, \ \ \widetilde{\gamma}_1(x) = \rho, \ q = 1\right\} \end{aligned}$$

and

$$G_q(x) = \begin{cases} \{1\} & \text{if} \quad q = 0, \ \widetilde{\gamma}_0(x) \geq \rho \\ \{0,1\} & \text{if} \quad \gamma_0(x) \geq \rho, \ \gamma_1(x) \geq \rho \\ \{0\} & \text{if} \quad q = 1, \ \widetilde{\gamma}_1(x) \geq \rho \end{cases}$$

Theorem IV.7. *Under the assumptions of Theorem IV.5, there exists $\beta \in \mathcal{KL}$ such that, for each $\varepsilon > 0$ and each compact set $K \subset \mathbb{R}^2$, there exists $\rho^* > 0$ guaranteeing the following property: for each $\rho \in (0, \rho^*]$ every solution $\chi = (x,q)$ to $\mathcal{H}^\rho$ with $\chi(0,0) \in K \times \{0,1\}$ is such that its x component satisfies*

$$|x(t,j)|_{\mathcal{A}_x} \leq \beta(|x(0,0)|_{\mathcal{A}_x}, t+j) + \varepsilon \quad \forall (t,j) \in \operatorname{dom}\chi \tag{33}$$

The proof follows analogously to the proof of Theorem IV.6. The property asserted by Theorem IV.7 will be illustrated numerically in Section V-C. A similar result can be obtained using temporal regularization.

For the spatially regularized control algorithm, no Zeno behavior occurs and certainly no "eventually discrete" solutions (in the sense of the solution that after some time t only jumps) exist due to the uniformly finite (nonzero) separation between the flow and jump sets–this property follows from [22, Lemma 2.7] since the closed-loop system satisfies the properties listed in Proposition IV.2.

V. Simulation results

In this section, we present several simulation results. First, in Section V-A, the closed-loop system $\mathcal{H}$ is simulated. Afterwards, the closed-loop system with general perturbations is simulated in Section V-B. Next, due to undesirable chattering, the spatially regularized system $\mathcal{H}^\rho$ is simulated in Section V-C. Afterwards, in Section V-D, simulations are performed to show how the system can enter the discontinuous conduction mode. In Section V-E, simulations are performed with changes in supply and demand of the Boost converter. The simulations are performed using $E = 5$V, $R = 3\Omega$, $c = 0.1$F, $L = 0.2$H, $P = \begin{bmatrix} \frac{c}{2} & 0 \\ 0 & \frac{L}{2} \end{bmatrix}$, and $x^* = (7,\ 3.27)$, unless noted otherwise. We used the Hybrid Equations Toolbox [24] for performing the simulations.

A. Simulating the closed-loop system

The simulation results for the closed-loop system $\mathcal{H}$ with initial conditions $x_0 = (0,5)$ and $x_0 = (5,0)$, for $K_0 = 0.05$ and $K_1 = 0.12$ are shown in Figure 5. As can be seen, the solutions converge from both initial conditions to the set $\mathcal{A}$ in correspondence with Theorem IV.5.

If we now change the desired setpoint $x^* = (v_c^*, i_L^*)$, which is only a parameter chance, the CLF and its derivative change

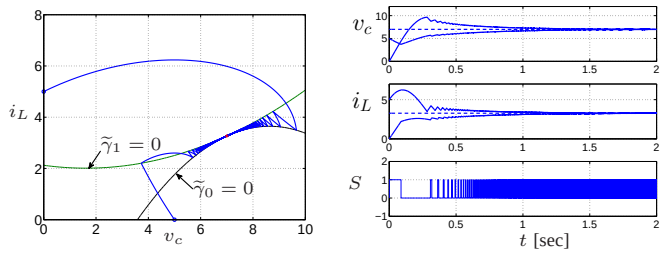

Fig. 5. Simulation results for the closed-loop system $\mathcal{H}$ with initial conditions $x_0 = (0, 5)$, $q_0 = 0$ and $x_0 = (5, 0)$, $q_0 = 1$, using $K_0 = 0.05$, $K_1 = 0.12$, and where S is only drawn for the simulation using $x_0 = (0, 5)$.

accordingly, and therefore also the control law. A simulation for the system with initial condition $x_0 = (3,\ 0)$, $K_0 = 0.12$, $K_1 = 0.08$, and desired output $v_c^* = 9$V and $i_L^* = 5.4$A is shown in Figure 6.

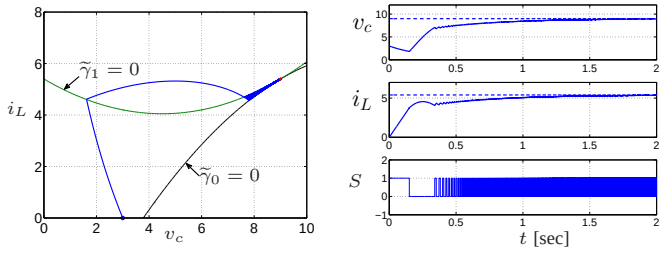

Fig. 6. Simulation results with initial conditions $x_0 = (0, 3)$, $q_0 = 1$, when $x^* = (9, 5.4)$, $K_0 = 0.12$, and $K_1 = 0.08$, starting in the set C.

As mentioned at the end of Section IV-D, the closed-loop system is robust to slowly varying parameters. To illustrate this, a simulation is performed with a dynamically changing set point x^* and adapting the CLF according to the changing set-point (the control law is modified accordingly). Initially, $x^* = (7, 3.27)$, but when this value is reached, we linearly increase x^* from $(7, 3.27)$ to $(10, 6.67)$. This simulation is shown in Figure 7. As it can be seen, the CLF can adapt to slow changes in the setpoint. Furthermore, the Boost converter follows the reference well and eventually reaches the final setpoint $x^* = (10, 6.67)$.

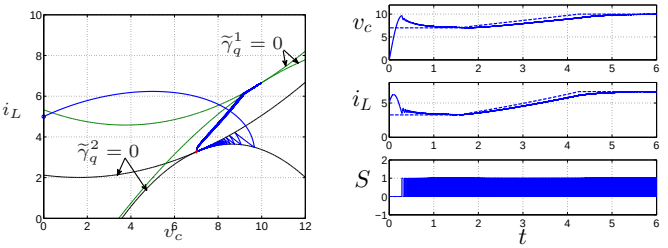

Fig. 7. Simulation results with initial conditions $x_0 = (5, 0)$, $q_0 = 0$, $K_0 = 0.05$, $K_1 = 0.12$, when x^* linearly changes from $(7, 3.27)$ to $(10, 6.67)$ and where K_0 and K_1 change to 0.07, where the black and green curves denote the switching boundaries for $x^* = (7, 3.27)$ and $x^* = (10, 6.67)$, respectively.

B. Simulating the closed-loop system with general perturbations

The perturbed closed-loop system $\widetilde{\mathcal{H}}$ is simulated, using $K_0 = 0.28$, $K_1 = 0.23$, and a sinusoidal perturbation injected in the state x, resulting in $d_1 = 0.5\sin(500t)$ and $d_2 = 0$ in (30). The results for initial conditions $x_0 = (8, 5)$ are shown in Figure 8. The Boost converter reaches a neighborhood of x^* and remains fluctuating due to the presence of the perturbation.

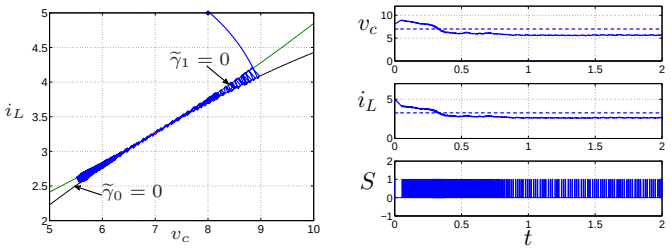

Fig. 8. Simulation results for the perturbed closed-loop system $\widetilde{\mathcal{H}}$ with $\delta = 0.5$, $K_0 = 0.28$, and $K_1 = 0.23$ for initial conditions $x_0 = (8, 5)$, $q_0 = 1$.

To provide insight on the results in Theorem IV.6, more simulations are performed in order to find a relationship between the maximal perturbation parameter δ (for the indicated sinusoidal perturbation, and where $(d_1, 0), (d_2, 0) \in \delta\mathbb{B}$) and the ball radius $\widetilde{\varepsilon}$, which is defined as the size of the ball where the steady state values converge to (for v_c and i_L), see (31) in Theorem IV.6. Note that in this simulation δ is used to find a value of $\widetilde{\varepsilon}$. The value of $\widetilde{\varepsilon}$ is approximated for various initial conditions (and the same sinusoidal perturbation using different values of d_1) using

$$\widetilde{\varepsilon} = \lim_{t+j\to\infty} \sup \sqrt{(v_c(t,j) - v_c^*)^2 + (i_L(t,j) - i_L^*)^2} \quad (34)$$

In particular here Theorem IV.6 indicates δ exists.

TABLE I
SIMULATION RESULTS FOR DIFFERENT VALUES OF ε.

δ	$v_c(t,j)$	$i_L(t,j)$	$\widetilde{\varepsilon}$	$\widetilde{\varepsilon}/\delta^{0.3}$
0.01	6.483	3.025	0.571	2.27
0.05	5.682	2.890	1.371	3.37
0.1	5.345	2.532	1.811	3.61
0.25	5.152	2.438	2.025	3.07
0.5	4.808	2.313	2.391	2.94
1	4.116	2.123	3.103	3.10

From the simulation results shown in Table I, where $v_c(t,j)$ and $i_L(t,j)$ denote typical values observed for large t and j where the system reached its steady state behavior,the relation between δ and $\widetilde{\varepsilon}$ can now be approximated specifically for $x^* = (7, 3.27)$, as

$$\widetilde{\varepsilon} \approx 3\delta^{0.3}$$

C. Simulating the spatially regularized closed-loop system

Now, the spatially regularized closed-loop system $\mathcal{H}^\rho$ is simulated. The results for initial conditions $x_0 = (0, 5)$, $q_0 = 1$ and $x_0 = (5, 0)$, $q_0 = 0$ for $K_0 = 0.28$ and $K_1 = 0.12$ are shown in Figure 9. To validate Theorem IV.7, more simulations are performed (using $K_0 = 0.7$ and $K_1 = 0.1$) in order to find a relationship between the regularization parameter ρ and the deviation from the equilibrium given by ε in Theorem IV.7 (similarly as in section V-B, see (34)).

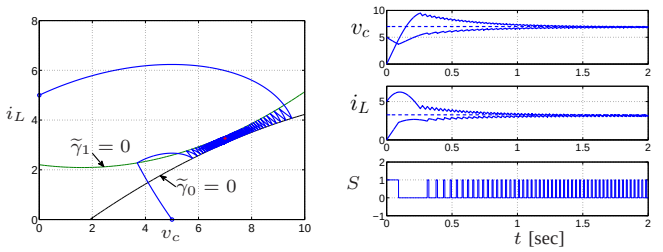

Fig. 9. Simulation results for the spatially regularized closed-loop system $\mathcal{H}^\rho$ with $\rho = 0.2$, $K_0 = 0.28$, and $K_1 = 0.12$ for initial conditions $x_0 = (0, 5)$, $q_0 = 1$ and $x_0 = (5, 0)$, $q_0 = 0$, and where S is only drawn for the simulation using $x_0 = (5, 0)$.

TABLE II
SIMULATION RESULTS FOR DIFFERENT VALUES OF ρ.

ρ	$v_c(t,j)$	$i_L(t,j)$	ε	ε/ρ	#SWs
0.01	6.989	3.259	0.013	1.34	1260
0.05	6.951	3.232	0.060	1.20	277
0.1	6.926	3.164	0.127	1.27	140
0.25	6.717	3.026	0.372	1.49	54
0.5	6.520	2.977	0.561	1.12	26

From the simulation results shown in Table II, the relationship between ρ and ε, specifically for $x^* = (7, 3.27)$, can now be approximated as $\varepsilon \approx 1.3\rho$. The last column of the table shows the number of switches per second over the same time horizon when a neighborhood of the set $\mathcal{A}$ is reached. As can be seen, the switching rate is reduced significantly by increasing the spatial regularization parameter ρ.

From the simulation results, the relationship between ρ and ε, specifically for $x^* = (7, 3.27)$, can now be approximated as $\varepsilon \approx 1.3\rho$.

Simulations for different values of ρ and different initial conditions are shown in Figure 10. As it can be seen, the larger the spatial regularization (the larger ρ) the larger the steady state error will be, as expected. Furthermore, the switching rate is reduced significantly by increasing the spatial regularization parameter ρ. Eventually, when ρ becomes too large, the controller may not be able to stabilize (a small regio around) the desired point x^* any longer.

D. Simulating the discontinuous conduction mode

In the next simulation we show how the system can enter the discontinuous conduction mode, thereby illustrating the relevance of the employed model including this mode explicitly; see [25]. The system parameters are now $E = 3$V, $R = 3\Omega$, and $x^* = (4, 1.78)$. In Figure 11, the simulation results for $\rho = 0.1$, $K_0 = 0.22$, and $K_1 = 0.13$ are shown. As can be seen, the system starts in mode 1 until i_L becomes zero, whereafter the system switches to mode 3. Next, the system remains in mode 3 until it hits the boundary $\widetilde{\gamma}_0(x) = \rho$ and switches to mode 2. Afterwards, switching between mode 1 and mode 2 occurs and a neighborhood of the point x^* is reached. Note that the closed-loop system works for a certain time period in the discontinuous conduction mode, showing the importance to include this mode in the overall model and global stability analysis.

E. Robustness to changes in supply and demand

The input voltage E and load R are now varied to assess the robustness of the spatially regularized control strategy to

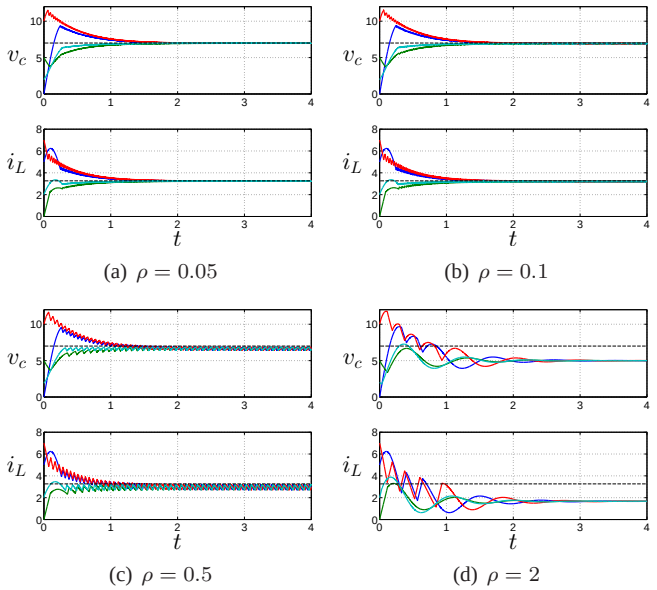

Fig. 10. Simulation results using different spatial regularization ρ for different initial conditions and $x^* = (7, 3.27)$, using $K_0 = 0.33$ and $K_1 = 0.12$.

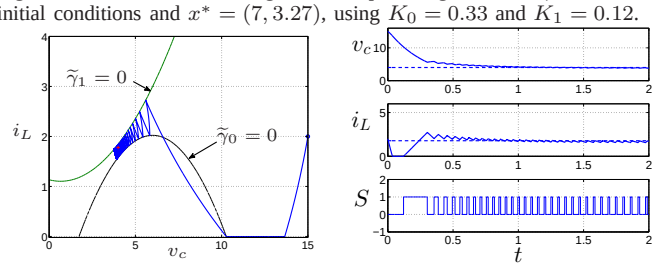

Fig. 11. Simulation results for $E = 3$V, $R = 3\Omega$, $\rho = 0.1$, $K_0 = 0.22$, and $K_1 = 0.13$, for initial condition $x_0 = (15, 2)$, $q_0 = 0$ and $x^* = (4, 1.78)$.

such changes. During the next simulation, the controller is observing the changes in E and R and is adapting accordingly, i.e., i_L^*, E and R are now time-varying in the CLF. Figure 12 shows a simulation where E is increased after 2 seconds from 2.5V to 5V and R is decreased after 4 seconds from 3Ω to 2Ω, the switching boundaries for the three different situations are shown as well. As it can be seen, a neighborhood of v_c^* is reached in all three situations, which means that the controller is able to cope with variations in the supply E and demand R.

In the next simulation, again input voltage E and load R are varied, but now the CLF/controller is not observing these variations, consequently, the controller is based on a constant $E = 5$V and $R = 3\Omega$. During the simulation, E is decreased after 2 seconds from 5 to 4V, and after 4 seconds back to 4V, R is decreased after 6 seconds from 3 to 2.5Ω, and after 8 seconds increased to 3Ω again. As can be seen in Figure 13, the solutions converge to a neighborhood of the set $\mathcal{A}$, however the performance decreases when the E and R are not identical to the parameters used for the CLF. Hence, adapting the controller to measured fluctuations in supply E and demand R is certainly beneficial.

VI. CONCLUSIONS

In this paper, a hybrid system approach to the control of the Boost converter was presented. First of all, a constrained switched system model with discontinuous right-hand side for all the modes was derived (including the discontinuous

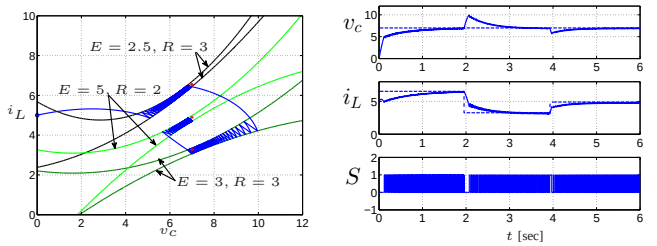

Fig. 12. Simulation results for a varying input voltage E and a varying load R with an adapting CLF and $\rho = 0.5$, $K_0 = 0.56/0.28/0.42$, and $K_1 = 0.05/0.12/0.18$, respectively, for initial condition $x_0 = (0, 5)$, $q_0 = 0$.

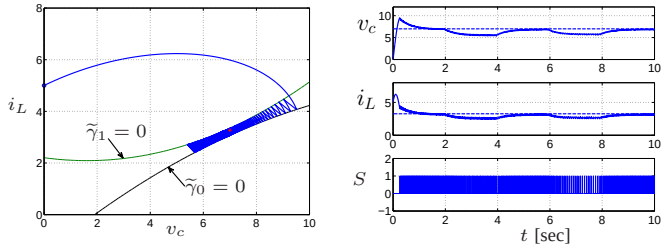

Fig. 13. Simulation results for a varying input voltage E and a varying load R with a constant CLF and $\rho = 0.5$, $K_0 = 0.28$, and $K_1 = 0.12$ for initial condition $x_0 = (0, 5)$, $q_0 = 0$.

conduction mode). For this model, a suitable Krasovskii regularization was determined, leading to a constrained switched differential inclusion. Based on this modeling setup a control Lyapunov function-based control design procedure was proposed. By formalizing the control setup in the hybrid systems framework of [14] and establishing important basic properties of the control scheme, various indispensable stability and robustness properties of the closed-loop system were derived. This is the first time that these essential properties are formally established for this electrical circuit. This article demonstrates the importance of hybrid systems tools for the analysis of the DC-DC Boost converter. The same tools can be used for the study of other converters. We hope the presented results stimulate the use of hybrid system tools for the analysis of general power systems.

Future work will involve the investigation of the state-dependent switching control law using the hybrid system framework for other type of converters.

Appendix A
Proof of Lemma III.3

To show *(b)*, note that we can rewrite (22) and (23) as

$$\gamma_0(x) = \widetilde{\gamma}_0(x) - K_0 \left(v_c - v_c^*\right)^2$$
$$\gamma_1(x) = \widetilde{\gamma}_1(x) - K_1 \left(v_c - v_c^*\right)^2$$

Because $K_0, K_1 > 0$, $\widetilde{\gamma}_q(x) \leq 0$ implies $\gamma_q(x) < 0$ if $v_c \neq v_c^*$.

If $v_c = v_c^*$ and $i_L \neq i_L^*$ (as otherwise $x = x^*$), we have $\widetilde{\gamma}_q(x) = \gamma_q(x) \leq 0$. However, we know that $\widetilde{\gamma}_q(x) = \gamma_q(x) = 0$ cannot occur, as together with $v_c = v_c^*$ this would imply $i_L = i_L^*$, which would be a contradiction. Hence, also in this case $\widetilde{\gamma}_q(x) = \gamma_q(x) < 0$, and the proof of property *(b)* is complete.

The proof of *(a)* follows analogously to the proof of lemma III.1. First define

$$\widetilde{\gamma}_0(x) = \gamma_0(x) + K_0 \left(v_c - v_c^*\right)^2 = \gamma_0(x) + K_0\delta_0(v_c) \quad (35)$$
$$\widetilde{\gamma}_1(x) = \gamma_1(x) + K_1 \left(v_c - v_c^*\right)^2 = \gamma_1(x) + K_1\delta_1(v_c) \quad (36)$$

we consider the sets $\widetilde{\Gamma}_q := \{x \in \mathbb{R}^2 \ : \ \widetilde{\gamma}_q(x) < 0\}$ for $q \in \{0, 1\}$. We will also use the boundaries of the sets $\widetilde{\Gamma}_q$ given by $\widetilde{\Omega}_q := \{x \in \mathbb{R}^2 \ : \ \widetilde{\gamma}_q(x) = 0\}$ for $q \in \{0, 1\}$, which are parabolas. Now define $\widetilde{\Gamma}_0$ and $\widetilde{\Gamma}_1$ by deriving (35) and (36) in similar forms as in (17) and (18)

$$\widetilde{\Gamma}_0 = \Bigg\{(v_c, i_L) \in \mathbb{R}^2 \ : \ i_L > \frac{1}{E - v_c^*} \left(\frac{1}{R}v_c^2 - \left(\frac{v_c^*}{R} + i_L^*\right) v_c + i_L^* E + K_0\delta_0(v_c)\right)\Bigg\} \quad (37)$$

$$\widetilde{\Gamma}_1 = \Bigg\{(v_c, i_L) \in \mathbb{R}^2 \ : \ i_L < \frac{1}{RE}v_c^2 - \frac{v_c^*}{RE}v_c + i_L^* + \frac{K_1\delta_1(v_c)}{E}\Bigg\} \quad (38)$$

and similar ones for $\widetilde{\Omega}_q$, $q \in \{0, 1\}$. Both parabolas $\widetilde{\Omega}_q$, $q \in \{0, 1\}$, have their axis of symmetry parallel to the i_L-axis. Then, because $\frac{1}{(E - v_c^*)} < 0, K_0\delta_0(v_c) > 0$, and Ω_0 is a "downward" parabola, we know that $\widetilde{\Omega}_0$ is also a "downward" parabola (it has a maximum in i_L-direction) and $\widetilde{\Gamma}_0$ is the region above it. Similarly, since Ω_1 is an "upward" parabola and $\frac{K_1\delta_1(v_c)}{E} > 0$, we have $\widetilde{\Omega}_1$ is also an "upward" parabola (it has a minimum in i_L-direction) and $\widetilde{\Gamma}_1$ is the region below it. If we now can show that $\widetilde{\Omega}_0 \cap \widetilde{\Omega}_1 = \mathcal{A}_x$, then it follows that $\widetilde{\Gamma}_1 \cup \widetilde{\Gamma}_2 = \mathbb{R}^2 \setminus \mathcal{A}_x$.

To show that $\widetilde{\Omega}_0 \cap \widetilde{\Omega}_1 = \mathcal{A}_x$, we find out the v_c, i_L value for the intersection of the two curves $\widetilde{\Omega}_0$ and $\widetilde{\Omega}_1$. When the right-hand-side of the inequalities in (37) and (38) equals to each other, we get a similar expression to (19):

$$\frac{1}{E - v_c^*}\left(\frac{1}{R}v_c^2 - \left(\frac{v_c^*}{R} + i_L^*\right) v_c + i_L^* E + K_0\delta_0(v_c)\right) = \frac{1}{RE}v_c^2 - \frac{v_c^*}{RE}v_c + i_L^* + \frac{K_1\delta_1(v_c)}{E}. \quad (39)$$

Then, we can rewrite (39) in quadratic form, and find its simplified discriminant Δ to be $\left(\frac{{v_c^*}^2}{RE}\right)^2 - {i_L^*}^2$, which equals to zero because $i_L^* = \frac{{v_c^*}^2}{RE}$. Therefore (39) has a unique solution. We can find the unique solution by solving v_c from (39), and the result is

$$v_c = \frac{-\left(\left(\frac{1}{R} - \frac{E - {v_c}^*}{RE} + 2K_0 - \frac{2K_1(E - v_c^*)}{E}\right) v_c^* + {i_L}^*\right)}{2\left(\frac{E - {v_c}^*}{RE} - \frac{1}{R} - K_0 + \frac{K_1(E - v_c^*)}{E}\right)} = v_c^*$$

while $i_L = i_L^*$. This implies that $\widetilde{\Omega}_0 \cap \widetilde{\Omega}_1$ is the set-point $\{(v_c^*, i_L^*)\}$ and therefore completes the proof of property *(a)*.

Property *(c)* can be shown by explicitly computing the limits. For finding the limit of the first two equations, we can rewrite the formulation of $\gamma_q(x)$ with $q \in \{0, 1\}$ as

$$\gamma_q(x) = (1 - q)\gamma_0(x) + q\gamma_1(x) = -\alpha(v_c - v_c^*)^2 + (\beta q + C_0)\left(-\frac{2i_L^*}{v_c^*}v_c + 2i_L\right)$$

where $\alpha = \frac{2p_{11}}{Rc}$, $\beta = \frac{p_{11}v_c^*}{c}$ and C_0 is given in the proof for Lemma III.1. Then, we get an expression

$$\widetilde{\gamma}_q(x) = (K_q - \alpha)(v_c - v_c^*)^2 + (\beta q + C_0)\left(-\frac{2i_L^*}{v_c^*}v_c + 2i_L\right) \quad (40)$$

We discuss the following cases when $K_q \to \alpha$,

- if $q=0$, we have the limit of (40) expression as

$$\lim_{K_0\to\alpha}\widetilde{\gamma}_q(x)=C_0\left(-\frac{2i_L^*}{v_c^*}v_c+2i_L\right).$$

- if $q=1$, we have the limit of (40) expression as

$$\begin{aligned}\lim_{K_1\to\alpha}\widetilde{\gamma}_q(x)&=(\beta+C_0)\left(-\frac{2i_L^*}{v_c^*}v_c+2i_L\right)\\&=\frac{p_{11}E}{c}\left(-\frac{2i_L^*}{v_c^*}v_c+2i_L\right)\\&=C_1\left(-\frac{2i_L^*}{v_c^*}v_c+2i_L\right).\end{aligned}$$

Thus, we complete the proof for the first two limits, and the last two limits follow naturally from the expression $\widetilde{\gamma}_q(x)=\gamma_q(x)+K_q(v_c-v_c^*)^2$.

APPENDIX B
PROOF OF PROPOSITION IV.2

Proof. We apply Proposition IV.1. First we check the viability condition (VC), which requires verifying that for each $(x,q)\in C\setminus D$, there exists a neighborhood U of (x,q) such that

$$F(\overline{x},\overline{q})\cap T_C(\overline{x},\overline{q})\neq\emptyset\qquad\forall(\overline{x},\overline{q})\in U\cap C\qquad(41)$$

In fact, note that if $(x,q)\in C\setminus D$, then for any sufficiently small neighborhood U of (x,q), it holds that $(\overline{x},\overline{q})\in U\cap C$ implies $(\bar{x},\bar{q})\in C\setminus D$ due to continuity of $\widetilde{\gamma}_S$, $S\in\{0,1\}$. Therefore, it suffices to show that (we dropped the bars in $\overline{x},\overline{q}$)

$$F(x,q)\cap T_C(x,q)\neq\emptyset\qquad\forall(x,q)\in C\setminus D\qquad(42)$$

To do so, we will first compute the tangent cones $T_C(x,q)$ for the set C as defined just below (24) for $(x,q)\in C\setminus D$:

- $q=0,\ i_L>0$: $T_C(x,q)=\mathbb{R}^2\times\{0\}$
- $q=0,\ i_L=0$: $T_C(x,q)=\mathbb{R}\times\mathbb{R}_+\times\{0\}$
- $q=1,\ v_c>0$: $T_C(x,q)=\mathbb{R}^2\times\{0\}$
- $q=1,\ v_c=0$: $T_C(x,q)=\mathbb{R}_+\times\mathbb{R}\times\{0\}$

Using these calculations, we have the following:

1) For $(x,q)\in C\setminus D$ such that $q=0$, $i_L>0$, (41) trivially holds.
2) For $(x,q)\in C\setminus D$ such that $q=0$, $i_L=0$, we have to distinguish two cases based on different set-valued vector fields in (2) depending if $x\in\overline{M_1}\setminus\overline{M_3}$ (i.e. $v_c<E$) or $x\in\overline{M_3}$ (i.e. $v_C\geq E$).
   a) If $x\in\overline{M_1}\setminus\overline{M_3}$ and thus $v_c<E$, we have the vector field
   $$\begin{pmatrix}f_a(x)\\0\end{pmatrix}=\begin{pmatrix}-\frac{1}{Rc}v_c+\frac{1}{c}i_L\\-\frac{1}{L}v_c+\frac{E}{L}\\0\end{pmatrix}\in T_C(x,q)$$
   because $-\frac{1}{L}v_c+\frac{E}{L}>0$.
   b) When $x\in M_3$ and thus $v_c>E$, we have a set-valued vector field (see (2)) given by
   $$\left\{-\frac{1}{Rc}v_c\right\}\times\left[-\frac{1}{L}v_c+\frac{E}{L},\ 0\right]\times\{0\}$$
   Since $(-\frac{1}{Rc}v_c,0,0)$ is an element of the set above and also lies in $T_C(x,q)$, (2) holds.
3) For $(x,q)\in C\setminus D$ such that $q=1$, $v_c>0$, (41) trivially holds.
4) For $(x,q)\in C\setminus D$ such that $q=1$, $v_c=0$, the vector field is given by $F_1(x)\times\{0\}$ that only contains the element $(0,\frac{E}{L},0)$ (see (3)), which lies in $T_C(x,q)=\mathbb{R}_+\times\mathbb{R}\times\{0\}$. Hence, (42) holds.

In summary, for each $\xi\in C\setminus D$, there exists a neighborhood U of ξ such that (41) holds. Thus, according to Proposition IV.1, there exists a nontrivial solution χ to $\mathcal{H}$ for points in $C\cup D$.

Now, to show that every maximal solution χ is complete, we prove that cases (b) and (c) in Proposition IV.1 cannot hold, and hence, only case (a) can be true.

Case (b) (finite escape time) cannot happen due to the fact that every maximal solution χ is bounded. Indeed, using lemma III.1 and property *(b)* of lemma III.3, the function V in (4), along a maximal solution χ, has non-positive derivative for flows and non-positive changes at jumps. Since V is quadratic it upper bounds the norm of the state (relative to the desired set point) and has compact sub-level sets. Therefore, $\lim_{t\to T}|\chi(t,j)|\leq M<\infty$ for some constant M and $T=\sup_t\text{dom}\chi$.

Case (c) (solutions jumping outside $C\cup D$[4]) can be excluded as well, because below we will show that $G(D)\subset C$, and thus $G(D)\subset C\cup D$.

In fact, to complete the proof we establish now that $G(D)\subset C$ and we consider two situations: I. $x\in D$ and $q=0$, and II. $x\in D$ and $q=1$.

I. Let $x\in D$ and $q=0$, and thus $\widetilde{\gamma}_0(x)=0$ and $x\in\widetilde{M_0}$ (i.e. $i_L\geq 0$). We will first show that this implies that $x\in\widetilde{M_1}$ (i.e. $v_c\geq 0$), i.e.

$$\left.\begin{matrix}\widetilde{\gamma}_0(x)=0\\ i_L\geq 0\end{matrix}\right\}\Rightarrow v_c\geq 0\qquad(43)$$

This latter implication will follow from the fact that $\widetilde{\Omega}_0:=\{x\in\mathbb{R}^2\mid\widetilde{\gamma}_0(x)=0\}$ is a downward parabola and the fact that the minimal root $\min\{v_c\mid x\in\widetilde{\Omega}_0,i_L=0\}$ is non-negative. Indeed, since $\widetilde{\Omega}_0$ is a downward parabola, these two facts would give

$$\begin{aligned}\min\{v_c\mid x\in\widetilde{\Omega}_0,i_L\geq 0\}&=\min\{v_c\mid x\in\widetilde{\Omega}_0,i_L=0\}\\&\geq 0\end{aligned}$$

which is equivalent to (43).

To compute the minimal root, we can use the expression in (22), showing that the points $x=(v_c,i_L)$ with $\widetilde{\gamma}_0(x)=0$ ($x\in\widetilde{\Omega}_0$) and $i_L=0$ satisfy

$$i_L=-\frac{\widetilde{A}_0}{C_0}v_c^2-\frac{\widetilde{B}_0}{C_0}v_c-\frac{\widetilde{D}_0}{C_0}=0$$

where $\widetilde{A}_0=A_0+\frac{K_0}{2}$, $\widetilde{B}_0=B_0-K_0v_c^*$, and $\widetilde{D}_0=D_0+\frac{K_0}{2}v_c^{*2}$, which can be rewritten as

$$\left(v_c-\left(-\frac{\widetilde{B}_0}{2\widetilde{A}_0}\right)\right)^2=-\frac{\widetilde{D}_0}{\widetilde{A}_0}+\left(-\frac{\widetilde{B}_0}{2\widetilde{A}_0}\right)^2$$

Then, the roots $v_{c1,2}$ of the function $\widetilde{\gamma}_0(x)|_{i_L=0}$ are given

[4]Note that flowing outside $C\cup D$ is not possible due to the closedness of C and D as formulated in the hybrid basic conditions.

by

$$v_{c1,2} = -\frac{\widetilde{B}_0}{2\widetilde{A}_0} \pm \sqrt{-\frac{\widetilde{D}_0}{\widetilde{A}_0} + \left(-\frac{\widetilde{B}_0}{2\widetilde{A}_0}\right)^2}$$
$$= -\left(\frac{p_{11} + \frac{p_{11}}{E}v_c^* - RcK_0}{-2p_{11} + RcK_0}\right) v_c^* \pm$$
$$\sqrt{-(v_c^*)^2 + \left(-\left(\frac{p_{11} + \frac{p_{11}}{E}v_c^* - RcK_0}{-2p_{11} + RcK_0}\right) v_c^*\right)^2}$$

in terms of system constants. Because $v_c^* > E > 0$ and $K_0 \in (0, \frac{2p_{11}}{Rc})$, $\min\{v_{c1}, v_{c2}\} \geq 0$ as long as $-(v_c^*)^2 + \left(-\left(\frac{p_{11}+\frac{p_{11}}{E}v_c^* - RcK_0}{-2p_{11}+RcK_0}\right) v_c^*\right)^2 > 0$. The left-hand side of the inequality can be rewritten as

$$\left(\frac{\frac{p_{11}}{Rc}\left(1 - \frac{v_c^*}{E}\right)}{K_0 - \frac{2p_{11}}{Rc}}\right) {v_c^*}^2$$

which is always positive since conditions $v_c^* > E > 0$ and $K_0 \in (0, \frac{2p_{11}}{Rc})$. This establishes (43). Using now property *(a)* of Lemma III.3, and $\widetilde{\gamma}_0(x) = 0$, we know that $\widetilde{\gamma}_1(x) \leq 0$ and thus $G(x,0) = (x,1) \in C$.

II. Let $x \in D$ and $q = 1$, and thus $\widetilde{\gamma}_1(x) = 0$ and $x \in \widetilde{M}_1$ (i.e. $v_c \geq 0$). Similar to case I. we will first show that this implies that $x \in \widetilde{M}_0$ (i.e. $i_L \geq 0$), i.e.

$$\left.\begin{array}{l} \widetilde{\gamma}_1(x) = 0 \\ v_c \geq 0 \end{array}\right\} \Rightarrow i_L \geq 0 \tag{44}$$

To show this we compute $\min\{i_L \mid \widetilde{\gamma}_1(x) = 0, v_c \geq 0\}$ and show it is nonnegative. First we observe that $\widetilde{\Omega}_1 := \{x \in \mathbb{R}^2 \mid \widetilde{\gamma}_1(x) = 0\}$ is an upward parabola. Using the expression in (23), the points $x = (v_c, i_L)$ satisfying $\widetilde{\gamma}_1(x) = 0$ are given by

$$i_L = -\frac{\widetilde{A}_1}{C_1}v_c^2 - \frac{\widetilde{B}_1}{C_1}v_c - \frac{\widetilde{D}_1}{C_1}$$

where $\widetilde{A}_1 = A_1 + \frac{K_1}{2}$, $\widetilde{B}_1 = B_1 - K_1 v_c^*$, and $\widetilde{D}_1 = D_1 + \frac{K_1}{2}{v_c^*}^2$. The minimum value $i_{L\min} := \min\{i_L \mid \widetilde{\gamma}_1(x) = 0\}$ results in two cases, namely

$$i_{L\min,1} = \frac{\widetilde{B}_1^2 - 4\widetilde{A}_1\widetilde{D}_1}{4\widetilde{A}_1 C_1},\ v_{c\min,1} > 0,\ K_1 \in \left(0, \frac{p_{11}}{Rc}\right) \tag{45}$$

$$i_{L\min,2} = -\frac{\widetilde{D}_1}{C_1}, \quad v_{c\min,2} = 0, \quad K_1 \in \left[\frac{p_{11}}{Rc}, \frac{2p_{11}}{Rc}\right) \tag{46}$$

where $i_{L\min}$ is found by either the vertex of the parabola or at $v_c = 0$ due to the constraint $v_c \geq 0$, respectively. Substituting the expressions of $\widetilde{A}_1, \widetilde{B}_1, \widetilde{D}_1$ into the right-hand side of (45) and (46), we have

$$i_{L\min,1} = \frac{\widetilde{B}_1^2 - 4\widetilde{A}_1\widetilde{D}_1}{4\widetilde{A}_1 C_1} = \frac{(6p_{11} - 4K_1Rc)\,{v_c^*}^2}{4p_{11}RE\,(2p_{11} - K_1Rc)}$$

$$i_{L\min,2} = -\frac{\widetilde{D}_1}{C_1} = \frac{(2p_{11} - K_1Rc){v_c^*}^2}{2p_{11}RE}$$

Since $R, c, E, v_c^*, p_{11} > 0$, we obtain

$$i_{L\min} > 0$$

and thus $\min\{i_L \mid \widetilde{\gamma}_1(x) = 0, v_c \geq 0\} \geq \min\{i_L \mid \widetilde{\gamma}_1(x) = 0\} = i_{L\min} > 0$. This establishes (44). Using now property *(a)* of Lemma III.3 and $\widetilde{\gamma}_1(x) = 0$, we know that $\widetilde{\gamma}_0(x) \leq 0$ and thus $G(x,1) = (x,0) \in C$.

This completes the proof. □

REFERENCES

[1] T. A. F. Theunisse, J. Chai, R. Sanfelice, and W. Heemels, "Hybrid control of the boost converter: Robust global stabilization," in *Proceedings of the IEEE Conference on Decision and Control*, 2013, pp. 3635–3640.

[2] J. Carrasco, L. G. Franquelo, J. T. Bialasiewicz, E. Galvan, R. C. P. Guisado, M. A. M. Prats, J. I. Leon, and N. Moreno-Alfonso, "Power-electronic systems for the grid integration of renewable energy sources: A survey," *IEEE Transactions on Industrial Electronics*, vol. 53, pp. 1002–1016, 2006.

[3] F. Vasca and L. Iannelli, Eds., *Dynamics and Control of Switched Electronic Systems*, ser. Advances in Industrial Control. Springer, 2012.

[4] R. D. Middlebrook and S. Cuk, "A general unified approach to modelling switching-converter power stages," in *Power Electronics Specialists Conference*, 1976, pp. 18–34.

[5] G. Escobar, A. J. Van Der Schaft, and R. Ortega, "A hamiltonian viewpoint in the modeling of switching power converters," *Automatica*, vol. 35, no. 3, pp. 445–452, 1999.

[6] M. Senesky, G. Eirea, and T. Koo, "Hybrid modelling and control of power electronics," in *Hybrid Systems: Computation and Control*, ser. Lecture Notes in Computer Science. Springer Berlin Heidelberg, 2003, vol. 2623, pp. 450–465.

[7] J. Buisson, P. Richard, and H. Cormerais, "On the stabilisation of switching electrical power converters," in *Hybrid Systems: Computation and Control*, ser. Lecture Notes in Computer Science. Springer Berlin Heidelberg, 2005, vol. 3414, pp. 184–197.

[8] T. Geyer, G. Papafotiou, and M. Morari, "On the optimal control of switch-mode dc-dc converters," in *Hybrid Systems: Computation and Control*, ser. Lecture Notes in Computer Science. Springer Berlin Heidelberg, 2004, vol. 2993, pp. 342–356.

[9] M. Camlibel, W. Heemels, A. Van Der Schaft, and J. Schumacher, "Switched networks and complementarity," *IEEE Transactions on Circuits and Systems I: Fundamental Theory and Applications*, vol. 50, no. 8, pp. 1036–1046, 2003.

[10] W. Heemels, M. Camlibel, A. Van Der Schaft, and J. Schumacher, "On the dynamic analysis of piecewise linear networks," *IEEE Transactions on Circuits and Systems I: Fundamental Theory and Applications*, vol. 49, no. 3, pp. 315–327, 2002.

[11] W. Heemels, M. Camlibel, A. Schaft, and J. Schumacher, "Modelling, well-posedness, and stability of switched electrical networks," in *Hybrid Systems: Computation and Control*, ser. Lecture Notes in Computer Science. Springer Berlin Heidelberg, 2003, vol. 2623, pp. 249–266.

[12] R. Frasca, M. Camlibel, I. Goknar, L. Iannelli, and F. Vasca, "Linear passive networks with ideal switches: Consistent initial conditions and state discontinuities," *IEEE Transactions on Circuits and Systems I*, vol. 57, no. 12, pp. 3138–3151, 2010.

[13] F. Vasca, L. Iannelli, M. Camlibel, and R. Frasca, "A new perspective for modeling power electronics converters: Complementarity framework," *IEEE Transactions on Power Electronics*, vol. 24, no. 2, pp. 456–468, 2009.

[14] R. Goebel, R. G. Sanfelice, and A. R. Teel, *Hybrid Dynamical Systems: Modeling, Stability, and Robustness*. New Jersey: Princeton University Press, 2012.

[15] D. E. Schwarz, "Consistent initialization for index-2 differential algebraic equations and its application to circuit simulation," Ph.D. dissertation, 2000.

[16] D. Liberzon and S. Trenn, "Switched nonlinear differential algebraic equations: Solution theory, Lyapunov functions, and stability," *Automatica*, vol. 48, no. 5, pp. 954 – 963, 2012.

[17] N. Krasovskii and A. Subbotin, *Game-Theoretical Control Problems*. Springer-Verlag, 1988.

[18] R. Sanfelice, R. Goebel, and A. Teel, "Generalized solutions to hybrid dynamical systems," *ESAIM: Control, Optimisation and Calculus of Variations*, vol. 14, no. 4, pp. 699–724, 2008.

[19] E. D. Sontag, "A Lyapunov-like characterization of asymptotic controllability," *SIAM Journal on Control and Optimization*, vol. 21, pp. 462–471, 1983.

[20] R. G. Sanfelice and C. Prieur, "Uniting two output-feedback hybrid controllers with different objectives," in *Proc. 29th American Control Conference*, 2010, pp. 910–915.

[21] R. Rockafellar and R. J.-B. Wets, *Variational Analysis*. Berlin Heidelberg: Springer, 1998.

[22] R. G. Sanfelice, R. Goebel, and A. R. Teel, "Invariance principles for hybrid systems with connections to detectability and asymptotic stability," *IEEE Transactions on Automatic Control*, vol. 52, no. 12, pp. 2282–2297, 2007.

[23] R. Goebel and A. Teel, "Solutions to hybrid inclusions via set and graphical convergence with stability theory applications," *Automatica*, vol. 42, no. 4, pp. 573–587, 2006.
[24] R. G. Sanfelice, D. A. Copp, and P. Nanez, "A toolbox for simulation of hybrid systems in Matlab/Simulink: Hybrid Equations (HyEQ) Toolbox," in *Proceedings of Hybrid Systems: Computation and Control Conference*, 2013, pp. 101–106.
[25] V. Sessa, L. Iannelli, and F. Vasca, "A complementarity model for closed-loop power converters," *IEEE Transactions on Power Electronics*, vol. 57, pp. 6821–6835, 2014.

Thomas Theunisse received his M.S. degree in mechanical engineering from the Eindhoven University of Technology (TU/e). His research interests are in the area of hybrid control theory, networked and event-triggered control systems and constrained systems including model predictive control.

Jun Chai received her M.S. degree in mechanical engineering from the University of Arizona in 2014. She is an enrolled Ph.D. student and research assistant at the University of California at Santa Cruz in computer engineering since then. Her research interests are in the area of hybrid control theory and applications.

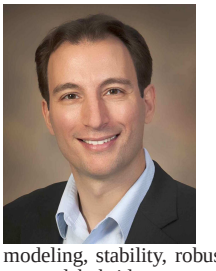

Ricardo G. Sanfelice is an Associate Professor at the Department of Computer Engineering at the University of California at Santa Cruz. He received his M.S. and Ph.D. degrees in 2004 and 2007, respectively, from the University of California at Santa Barbara. Prof. Sanfelice is the recipient of the 2013 SIAM Control and Systems Theory Prize, the National Science Foundation CAREER award, the Air Force Young Investigator Research Award, and the 2010 IEEE Control Systems Magazine Outstanding Paper Award. His research interests include modeling, stability, robust control, observer design, and simulation of nonlinear and hybrid systems with applications to power systems, aerospace, and biology.

Maurice Heemels is a Full Professor in the Control Systems Technology group (Mech. Eng.) of the Eindhoven University of Technology (TU/e). He held visiting research positions a.o. at the Swiss Federal Institute of Technology (ETH), Zurich, Switzerland, (2001) and at the University of California at Santa Barbara (2008). His current research interests include hybrid and cyber-physical systems, networked and event-triggered control systems and constrained systems including model predictive control.